Organic Geochemistry 129 (2019) 45–62

Contents lists available at ScienceDirect

Organic Geochemistry

journal homepage: www.elsevier.com/locate/orggeochem

Riverine mixing at the molecular scale – An ultrahigh-resolution mass spectrometry study on dissolved organic matter and selected metals in the Amazon confluence zone (Manaus, Brazil)

C. Simon [a,b], H. Osterholz [a], A. Koschinsky [c], T. Dittmar [a,d,*]

[a] Institute for Chemistry and Biology of Marine Environment (ICBM), ICBM-MPI Bridging Group for Marine Geochemistry, 26129 Oldenburg, Germany
[b] Max Planck Institute for Biogeochemistry, Molecular Biogeochemistry, 07745 Jena, Germany[1]
[c] Jacobs-University Bremen, Department of Physics and Earth Sciences, 28759 Bremen, Germany
[d] Helmholtz Institute for Functional Marine Biodiversity at the University of Oldenburg (HIFMB), 26129 Oldenburg, Germany

ARTICLE INFO

Article history:
Received 18 May 2018
Received in revised form 22 January 2019
Accepted 23 January 2019
Available online 25 January 2019

Keywords:
Water chemistry
Evolution
Chemical diversity
DOM
Complexation
Partitioning
Disequilibrium
Surface
Interface
FT-ICRMS
Trace metals

ABSTRACT

The Amazon delivers a fifth of the global continental runoff and riverine dissolved organic carbon (DOC) to the ocean. Intensified biogeochemical processes are expected at the junction of the Amazon's major blackwater tributary, the Rio Negro, and its parent, the Rio Solimões, due to large gradients in pH, conductivity, DOC and particle load. Dissolved organic matter (DOM) plays a major role in aquatic biogeochemical processes which are poorly understood on the molecular level. To gain insights into the potential role of DOM in non-conservative processes, we assessed dynamics of Cu, Fe and DOM by ultrahigh resolution mass spectrometry in: (1) endmembers, (2) regional samples and (3) laboratory mixing experiments under presence/absence of natural particles (>0.2 μm). The relative abundances of 3600 DOM molecular formulae were interpreted via multivariate statistics which revealed major dynamics in the DOM molecular composition. >40% of molecular formulae displayed conservative behavior even in the presence of natural particles, agreeing with bulk DOC behavior, but opposing the often-presumed non-conservative behavior of DOM. Another 16–27% of formulae fluctuated in FT-ICRMS signal intensity during mixing, but did not show consistent non-conservative behavior. Both rivers left a clear molecular imprint within the DOM of the Amazon, each being linked to >800 molecular formulae. Characteristic for the Rio Negro was a dominance of phenolics with a wide molecular mass range (centered at ~400 Da), and for the Rio Solimões more saturated but lower-molecular mass compounds (centered at ~300 Da). Both Fe and Cu showed distinct non-conservative mixing patterns under particle presence. In the controlled mixing experiments including original particles at natural concentration, up to 0.5 μg/L Cu was released from the particles into solution at 20–40% blackwater contribution. Our molecular analysis revealed distinct DOM compositional changes in polyphenol- and nitrogen-containing formulae paralleling this release, suggesting links to desorption of potential ligands and charge-induced effects at particle surfaces caused by pH and conductivity changes in the course of mixing.

© 2019 Elsevier Ltd. All rights reserved.

1. Introduction

Terrestrial aquatic systems – such as rivers, lakes and wetlands – act as transporters, storages and reactors of organic matter (Battin et al., 2009; Aufdenkampe et al., 2011; Abril et al., 2014). Rivers connect land surface and oceans, and their hydrology influences biogeochemical cycles of their various dissolved, colloidal, suspended and particulate constituents (Gaillardet et al., 2014).

Dissolved organic matter (DOM) forms a highly complex mixture of thousands of individual molecules interacting with other coexisting solutes and non-dissolved constituents (Kujawinski, 2011; Gonsior et al., 2016). DOM is both metabolic waste (lysis, exudation) and substrate to heterotrophs and thus represents an integral component of the food web (Longnecker et al., 2015). As such, it connects the chemical diversity of cell metabolism and chemical ecology (Kujawinski, 2011). DOM interacts with particles and colloids, either by sorption or desorption, and thus controls

* Corresponding author at: Institute for Chemistry and Biology of Marine Environment (ICBM), ICBM-MPI Bridging Group for Marine Geochemistry, 26129 Oldenburg, Germany.
E-mail address: thorsten.dittmar@uni-oldenburg.de (T. Dittmar).
[1] Present address.

https://doi.org/10.1016/j.orggeochem.2019.01.013
0146-6380/© 2019 Elsevier Ltd. All rights reserved.

surface charge properties through surface conditioning (Aufdenkampe et al., 2001; Avneri-Katz et al., 2017). It also interacts with small ions, such as trace metals, by complexation which in turn controls partitioning, bioavailability, and toxicity of those metals (Shank et al., 2004a; Fritsch et al., 2009). Finally, DOM is affected by a range of abiotic controls, such as photochemistry or redox chemistry that modify or induce the above interactions (Riedel et al., 2013; Waggoner et al., 2015; Johannsson et al., 2016; Waggoner and Hatcher, 2017).

Abrupt changes of environmental conditions, either in space ("hot spots", e.g., at interfaces connecting soils, wetlands, sediments and rivers) or time ("hot moments", e.g., during algal blooms or flooding events, or upon injection of easily degradable substrate) influence the dynamics of carbon pools in natural systems (Marín-Spiotta et al., 2014; Kuzyakov and Blagodatskaya, 2015; Ward et al., 2017). Mixing phenomena in aqueous media combine both spatial and temporal aspects in a unique way and occur in several settings in nature, most prominent at river confluences or at the boundary of riverine and marine systems.

Although there is a solid body of literature on biogeochemical processes and their effects on elementary mass balances at aquatic boundaries, most of this work has been conducted in estuaries. There is relatively little known about how physical mixing of different riverine water bodies and disequilibria that may evolve during this mixing process and its influence on DOM molecular composition. Most studies report non-conservative effects upon riverine mixing (i.e., deviating from simple dilution) which affect phase partitioning and are frequently linked to distinct changes in DOM composition (Table 1). Also, respiration (Mayorga et al., 2005; Abril et al., 2014) and variations in discharge or flow velocity (Loder and Reichard, 1981; Cifuentes et al., 1990; Asmala et al., 2016; Ward et al., 2018) must be taken into account as relevant processes during mixing (Ward et al., 2018).

Evolving disequilibria among the dissolved and solid constituents increase the probability of biogeochemical reactions taking place (McKnight et al., 1992; Mulholland et al., 2015; Guinoiseau et al., 2016), with further implications for food webs (Rice et al., 2008; Farjalla, 2014; Röpke et al., 2016). Dissolved organic compounds modify particle surfaces by conditioning (Davis, 1982; Brown and Calas, 2012) and thereby influence the partitioning of trace metals (Takahashi et al., 1999). For example, iron (Fe) and copper (Cu) are among the elements that show highest affinities towards organic matter (Xue and Sigg, 2002; Ksionzek et al., 2018). Metals are complexed by a suite of competing inorganic or organic ligands that control their bioavailability and toxicity, and there is evidence for the presence of highly specific organic ligands in aquatic systems especially regarding essential trace elements like Cu and Fe (Ross et al., 2000; Buck et al., 2012; Waska et al., 2015). However, knowledge about the nature or identity of these ligands within DOM remains scarce (Xue and Sigg, 2002; Gaillardet et al., 2014). A better constraint on the nature of the dissolved organic compounds involved in non-conservative effects and their link to trace metal complexation and sorption to particle surfaces is thus desired. Electrospray ionization (ESI) coupled to FT-ICRMS allows the study of the molecular composition of DOM in unprecedented detail, providing chemical information about thousands of resolved molecular masses (Koch et al., 2007; Kujawinski, 2011; Gonsior et al., 2016).

One of the largest freshwater confluences on earth is located at Manaus, Brazil (Encontro das Águas, 3.17°S, 59.96°W, Fig. 1), where the Rio Negro joins the Rio Solimões to form the Amazon River. Studying DOM dynamics in this system is of great interest for five reasons. First, the Amazon is the largest river in terms of catchment size (6.4×10^6 km^2) and annual discharge (6.6×10^{12} m^3), accounting for 16.5% of the global continental runoff (Coynel et al., 2005; Dai et al., 2012). Moreover, the Amazon delivers one-fifth of riverine dissolved organic carbon (DOC) to the ocean (being equal to a flux of $35 \pm 4 \times 10^6$ Tg C_{org}, with about 17% being contributed by the Rio Negro (Ertel et al., 1986; Coynel et al., 2005). Second, the Amazon system can be regarded as a relatively

Table 1
Summary of proposed processes and mechanistic explanations for non-conservative phenomena at freshwater confluences.

Agent	Process	Proposed explanatory mixing phenomena[a]	References[b]
DOM	Sorption	↑ Availability of surfaces (formed in situ)	[1], [2], [3], [4]
		↑ pH changes	
		DOM composition (see Fractionation)	
	Release	↑ Ion strength increase (abiotic hydrolysis rate of DOC/POC, from hydrolysable tannins)	[5]
		↑ Ion strength increase (salting-in of amphoteric compounds, mainly proteinaceous compounds)	
	Flocculation/coagulation	↑ Ion strength increase, decrease of electrostatic repulsion	[1], [2], [6]
		↑ Protonated sites on DOM	
	Fractionation, preferential sorption of DOM	Hydrophobic and aromatic moieties	[6], [7], [8], [9], [10]
		Nitrogen-containing compounds	
		Humic acids (over fulvic acids)	
		Molecules with greater aromaticity, carboxylic and amino acid moieties	
Particles	Sedimentation	↑ Velocity decrease	[1], [2], [7]
	Formation	↑ pH and ion strength increase (Kaolinite)	[1], [10], [11], [12]
		↑ Ion strength increase (SPM in general)	
		↑ Ion strength increase (Fe oxyhydroxides s.l.)	
		↑ pH increase (Fe, Al-oxyhydroxides)	
	Dissolution	See process column "Release" (→DOM,→ Metal ions in solution)	
Metal ions in solution	Release	↑ Ion strength increase (from OM complexes)	[2], [12]
		↑ Reductive dissolution (Mn oxides or outer-sphere complexes)	
		↑ Radical formation (from quinone moieties)	
		↑ Photochemical decay (of OM)	
	Sorption to solid particles	↑ Availability of surfaces (formed in-situ)	[1]
		↑ pH increase	
	Complexation	↑ pH and ion strength increase	[1], [2], [12]
		↓ Ion strength increase	

[a] No biotic factors included; e.g., increased respiration or exudation of DOM.
[b] References: [1] Guinoiseau et al. (2016), [2] Aucour et al. (2003), [3] Leenheer and Menezes Santos (1980), [4] McKnight et al. (1992), [5] Spitzy and Leenheer (1991), [6] Pérez et al. (2011), [7] Moreira-Turcq et al. (2003), [8] Aufdenkampe et al. (2001), [9] Ertel et al. (1986), [10] McKnight et al. (1992), [11] Merschel et al. (2017), [12] Mulholland et al. (2015).

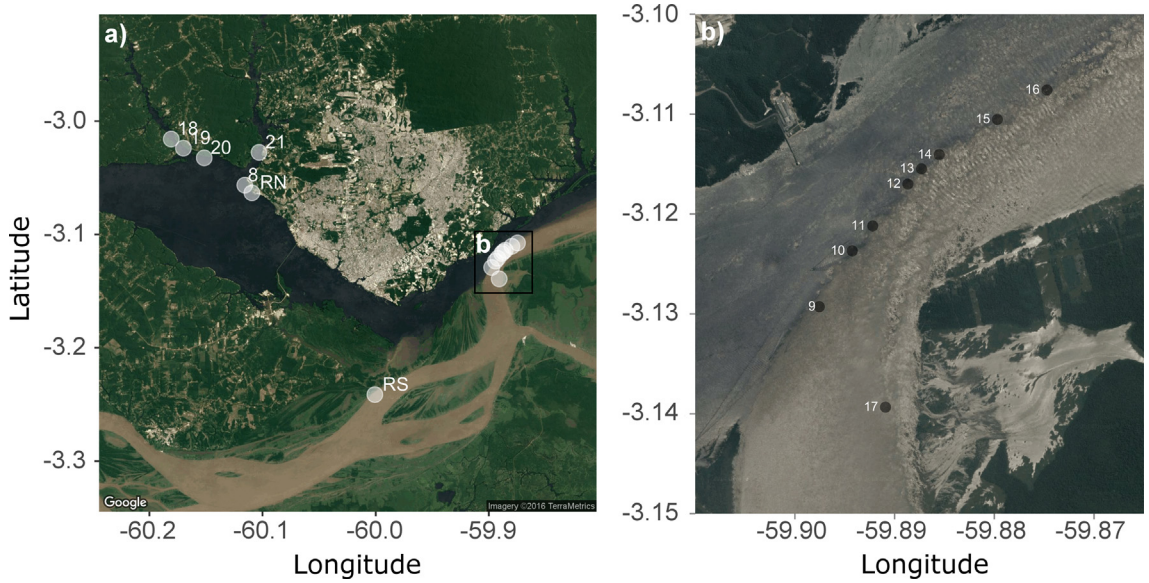

Fig. 1. (a) Surface water sampling locations. Samples RN and RS refer to endmembers used for laboratory mixing experiments; all other samples belong to the regional sample set (NAT). (b) Detail of (a) showing a close-up of the initial confluence zone. Map data accessed with ggmap v2.6.1 in RStudio v1.1.456 from Google Maps.

unperturbed river system and is thus especially suited for in situ studies (Furch and Junk, 1997; Devol and Hedges, 2001; Junk et al., 2011; Affonso et al., 2015). Third, intensified biogeochemical processes are expected in the confluence zone due to strong chemical gradients of pH (5–7.5), dissolved organic carbon (3–11 mg/L) and suspended particulate matter (<10–230 mg/L).

The large difference between the two rivers is due to contrasting properties of both river basins in terms of geology, climate, hydrology and erosion regime, vegetation, and ecosystem processes (Ertel et al., 1986; Furch and Junk, 1997; Quesada et al., 2011) producing whitewater (Solimões) and blackwater (Negro) rivers. Fourth, another important feature of the confluence is that the rivers do not completely mix over a course of up to 100 km (Laraque et al., 2009; Mulholland et al., 2015). This phenomenon has been attributed to differences in physical properties such as temperature and density, but also to differences in hydrology, such as flow velocity or streambed geometry (Furch and Junk, 1997; Laraque et al., 2009; Filizola et al., 2010; see Supplementary Note S1 for more references). Lastly, the large Amazon River network shows a high number of branching points and thus covers a wide range of stream orders (McClain and Elsenbeer, 2001) and is characterized by different climatic patterns that are integrated in a complex manner by the main stem of the river (Richey et al., 1989). The interplay of the network's structure and large-scale climate patterns governs the flood pulse (Furch and Junk, 1997; Vidal et al., 2015) that largely controls exchange between floodplains, wetlands and the mainstem (Viers et al., 2005; Junk et al., 2011; Mortillaro et al., 2011) and also influences fluxes and properties of the transported organic matter (Moreira-Turcq et al., 2003b, 2013).

To study the composition and reactivity of DOM and its interaction with trace metals, we investigated water samples from the Amazon confluence zone with ultrahigh resolution mass spectrometry and conducted controlled mixing experiments under the presence or absence of natural particles. Trace metal behavior was analyzed by using Fe and Cu. We focused on: (1) river endmember characterization (Rio Solimões/Rio Negro), (2) a set of samples from the actual mixing zone and regional small tributaries, and (3) controlled mixing experiments. We hypothesized that the non-conservative behavior of trace metals would be linked to the presence of particles and result in distinct molecular compositional changes in the DOM pool.

2. Materials and methods

2.1. Samples and experiments

River surface water samples from Rio Negro (RN) and Rio Solimões (RS) were taken in two sampling campaigns at the end of October 2013 and in July 2014. In 2013, both rivers (endmembers) and their direct mixing gradient were sampled (samples 08–17, Fig. 1, Table 2). Two smaller tributaries close to Manaus, the Rios Tarumã Mirim and Tarumã Açu were sampled as well (samples 18–21). Further details on flow conditions during the 2013 sampling are given in the Supplementary Note S1 in the Supplementary Material and Supplementary Figs. S1 and S2. Two additional endmember samples taken in 2014 were used for laboratory mixing experiments (RN and RS, Fig. 1).

In the following, the natural mixing sample set (NAT) refers to the 2013 samples and simulated mixing (MIX) refers to the 2014 samples. The MIX samples were further separated into "filtered" (F) and "non-filtered" (NF) samples based on the treatment of the endmember samples before mixing (Supplementary Tables S1 and S2; workflow given in Supplementary Fig. S3). NAT samples were filtered with sterile 0.2 µm cellulose acetate syringe filters (Sartorius Minisart NML, Sartorius, Göttingen, Germany), acidified to pH 2 (HCl, Ultrapur, Roth, Karlsruhe, Germany) immediately after sampling and stored in the dark (4 °C). Cellulose acetate was used instead of glass microfiber filters (e.g., GF/F) to prevent trace metal contamination. Conductivity was taken as a conservative measure of mixing (Moreira-Turcq et al., 2003a; Mulholland et al., 2015) in NAT samples (Table 2) and confirmed by concentrations of conservative cations (Na, Ca, Sr, Mo, etc.; Supplementary Fig. S4).

Sampling and storage of MIX endmember samples RS and RN followed the same procedures as described for NAT, with the only exception that samples were neither filtered nor acidified until processed to conduct controlled laboratory experiments in Bremen. Following the procedure given in Mulholland et al. (2015),

Table 2
Geochemical data of the NAT sample set. Abbreviations: ID, sample number; f, relative amount of Rio Negro endmember (1 = 100%); DOC, dissolved organic carbon; Cu and Fe, dissolved copper and iron; d.Cu, fraction of non-conservative dissolved copper; d.Fe, fraction of non-conservative dissolved iron; Cond., conductivity; T, temperature.

ID	f	DOC (±RSD) [mg/L]	Cu (±RSD[c]) [μg/L]	d.Cu [μg/L]	Fe [c] (±RSD) [μg/L]	d.Fe [μg/L]	Cond. [μS/cm]	O_2 [mg/L]	T [°C]	pH
08	1	7.3 ± 0.16	0.73[b]	0.0	198 ± 3.6	0	8.9	5.8	31.6	5.3
11	0.9	9.3 ± 0.21	0.78 ± 0.03[c]	−0.18	198 ± 3.6	10	16.1	5.8	31.2	6.2
12	0.77	7.2 ± 0.15	2.09[b]	0.83	159 ± 2.9	−18	25.0	6.2	30.9	6.1
14	0.6	6.2 ± 0.13	1.10 ± 0.04[c]	−0.52	191 ± 3.4	30	36.4	6.1	30.8	6.4
10	0.53	8.1 ± 0.17	1.49 ± 0.06[c]	−0.16	209 ± 3.8	55	41.4	6.6	30.9	6.6
13	0.37	5.7 ± 0.12	1.98 ± 0.08[c]	−0.17	129 ± 2.3	−10	52.5	6.2	30.8	6.2
15	0.17	4.6 ± 0.15	1.98 ± 0.08[c]	−0.52	145 ± 2.6	25	66.1	6.3	30.7	6.7
16	0.08	4.1 ± 0.13	1.97 ± 0.08[c]	−0.85	181 ± 3.3	70	72.9	6.4	30.6	6.8
09	0	3.8 ± 0.08	2.99[b]	0.0	104 ± 1.9	0	78.2	5.7	30.8	6.9
17	0[a]	4.6 ± 0.15	5.36 ± 0.21	–	240 ± 4.3	–	78.4	5.7	31.0	7.1
18	–	8.2 ± 0.26	0.53 ± 0.02[c]	–	119 ± 2.1	–	6.4	6.7	33.7	4.9
19	–	7.5 ± 0.24	0.95 ± 0.04[c]	–	126 ± 2.3	–	6.8	6.6	33.5	4.9
20	–	25.4 ± 0.82	4.38 ± 0.18[c]	–	174 ± 3.1	–	7.0	6.6	33.2	4.9
21	–	7.7 ± 0.25	1.37 ± 0.05[c]	–	115 ± 2.1	–	12.8	6.5	31.9	5.7

[a] Based on conductivity.
[b] Determined by CLE-AdCSV.
[c] Determined by ICPMS.

the position of the sample on the mixing gradient was expressed by the f-value which is the amount of Rio Negro water in % divided by 100. Mixing experiments with unfiltered endmembers ("MIX NF") were conducted directly after transport from Manaus to Bremen on July 28, 2014. Mixing of endmember samples was conducted in 10% steps (9 samples + both endmembers, no replicate treatments). Samples were allowed to equilibrate for 24 h on a shaker (at room temperature, 120 rpm, HS 260 basic, IKA-Werke GmbH & Co. KG, Staufen, Germany), filtered (0.2 μm syringe filters, Whatman Puradisc FP 30 cellulose acetate, GE Healthcare, Freiburg, Germany) and acidified as described above. These mixing conditions were similar to those in Merschel et al. (2017), working on similar samples.

Thereafter, 750 ml of the endmember samples were filtered (0.2 μm, cellulose acetate) and used for the second mixing experiment on August 5, 2014, yielding a third sample set ("MIX F"). The mixing conditions for the MIX F sample series were identical to the conditions for MIX NF (time, temperature, filtration, and acidification). The filters of the Rio Negro and Solimões endmembers were air-dried and kept for geochemical analysis to characterize the particulate matter interacting with the dissolved metals and DOM during the mixing (Supplementary Note S2).

2.2. Extraction of DOM and bulk analysis of carbon, copper and iron

Samples were extracted by solid phase extraction (SPE) on 100 mg modified styrene divinylbenzene polymer (Bond Elut, Agilent Technologies, Santa Clara, USA), following a published protocol (Dittmar et al., 2008). Applied sample volumes ranged from 3 to 8 ml, being higher for samples with lower DOC content. Each sample was extracted once. Extraction efficiencies determined for three samples (including both endmembers) were 58 ± 2%, 77 ± 6% and 82 ± 6% for MIX F, NAT and MIX NF, respectively. The extraction was done about one month before FT-ICRMS analysis. Until analysis, methanol extracts were stored in combusted amber vials with acid-rinsed Teflon liners at −20 °C in the dark.

Bulk analysis of dissolved organic carbon (DOC) was performed with a TOC analyzer (Shimadzu TOC-V_{CPH}, Kyoto, Japan). Detection limit was on average 0.12 mg C/L. Accuracy and precision were in the ±5% relative standard deviation range. The accuracy of the DOC determination was confirmed by analyzing a deep sea reference (DSR) material provided by Dennis Hansell (University of Miami). Procedural blanks were obtained with ultrapure water, considering all steps of sample preparation. Regular blanks (MIX NF, NAT) showed DOC levels of 0.18 mg C/L. MIX F samples (including an additional filtration step with cellulose acetate, 0.2 μm, before mixing) had slightly elevated levels of 0.48 mg C/L. These values were subtracted from the respective DOC concentration (Fig. 2a).

Copper and iron concentration were measured on a double-focusing ICPMS (Inductively Coupled Plasma Mass Spectrometer) with a reverse Nier-Johnson geometry (Element 2, Thermo Fisher Scientific, Waltham, USA). Analysis was conducted in low resolution (LR, $m/\Delta m = 600$, full width at half maximum) and mid resolution mode (MR, $m/\Delta m = 8000$). The analyzed isotopes (resolution mode in brackets) were ^{63}Cu (MR), ^{65}Cu (LR) and ^{56}Fe (MR). Samples (5 ml, acidified with HCl, pH 2) were spiked with internal standard (50 μl, ^{115}In). The lowest calibration point was taken as an estimate of the detection limit (1 μg/L Cu, 10 μg/L Fe). Values below this operational detection limit are not necessarily false or imprecise.

Precision and accuracy of Cu and Fe (checked with standard materials SLRS 4/SLRS 5, NRC-CNRC, Ottawa, Canada) determination were in the ±5% relative standard deviation range. Selected samples of the NAT set were also analyzed for total dissolved Copper (TDCu) and Cu-specific ligands by competitive ligand exchange-adsorptive cathodic stripping voltammetry and its reverse titration equivalent to assess Fe-specific ligands (CLE-AdCSV; Hawkes et al., 2013; Kleint et al., 2015; see Supplementary Note S3, Supplementary Fig. S5, and Supplementary Tables S3, S4 and S5). To estimate the fraction of non-conservative Fe and Cu ("d.Fe", "d.Cu"; Table 2, Supplementary Tables S1 and S2), the theoretical concentration (represented by the mixing line; expected in case of simple dilution) was subtracted from the measured concentration (yielding positive or negative anomalies).

2.3. Analysis of DOM molecular composition by FT-ICRMS

The extracts (including procedural blanks) were diluted to 20 mg C/L and refiltered (0.2 μm PTFE) one day before FT-ICRMS analysis. Ultrahigh-resolution mass spectrometry of SPE-DOM was conducted on an FT-ICRMS (15 T, Bruker solariX, Bremen, Germany) equipped with an electrospray ionization source (ESI, Apollo II) in negative ionization mode as described in Rossel et al. (2016). Each sample was injected once; instrumental stability was checked

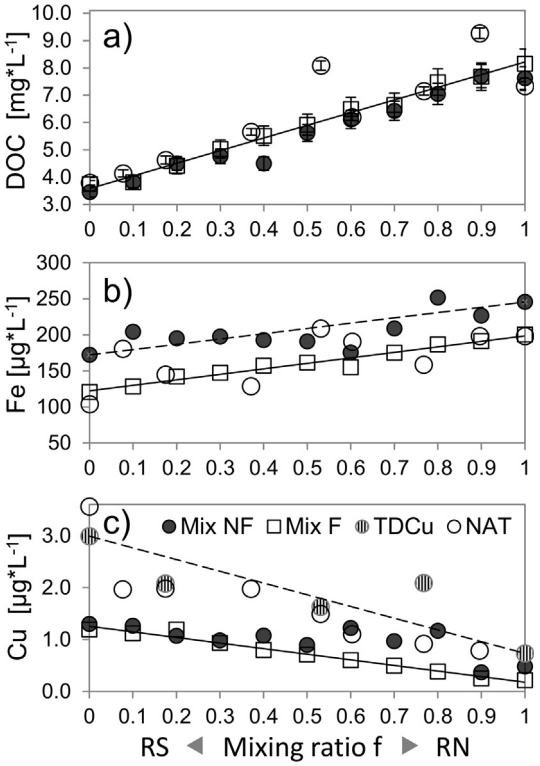

Fig. 2. Mixing plots of: (a) DOC, (b) Fe and (c) Cu for the three sample sets. Mixing ratio f refers to the amount of Rio Negro (RN) water in the sample mix (1 = 100%). The mixing set with absence of particles consistently shows conservative behavior (MIX F). Particles trigger non-conservative processes (MIX NF, NAT). SOL, Rio Solimões. As a reference, the linear trend of the MIX F data is shown as a solid line; for comparison, the linear trend of MIX NF is given in (b) as a dashed line. TDCu, total dissolved copper, determined by CLE-AdCSV for selected NAT samples.

with two reference samples. Source-induced dissociation (SID) at 40 eV was used to suppress dimer formation during ionization. All detected compounds had a molecular mass <650 Da. Mass spectra were internally recalibrated and aligned by in-house Matlab routines (Rossel et al., 2016). Peaks were considered reliable if they had an S/N ≥ 4 and were detected in more than one sample. Peaks that occurred at an S/N > 20 in procedural blanks were removed from further consideration in all samples (Riedel and Dittmar, 2014; Rossel et al., 2016). Finally, masses that were detected in <20% of the samples and had an S/N ratio of less than 20 were removed from the data set.

Molecular formula assignment included the elements C, H, N, O, P and S and was conducted at the following settings: $O_{min} = 1$, $C_{max} = 40$, $N_{max} = 4$, $S_{max} = 2$, $P_{max} = 1$, $O/C_{max} = 1$, $H/C_{min} = 0.3$. Post-processing followed the procedure given in Rossel et al. (2016). After performing all processing steps, the dataset contained 5980 masses with formulae assigned to 66.7% of them (n = 3982). The fraction of signal of non-assigned masses was highly similar across all samples in terms of number and ion abundance (18.1 ± 1.2% and 1498 ± 98; mean ± standard deviation, n = 36). ^{13}C isotopologues (1257 formulae in total) accounted for the majority of this information (10.1 ± 0.4% of signal, 1012 ± 35 masses; mean ± standard deviation, n = 36). The dataset used for multivariate statistical analysis ("core formulae dataset") contained only monoisotopic formulae that were present in (1) at least two samples per sample set, and (2) found in both MIX experiments, yielding a final set of 3608 formulae. This number is equivalent to 90% of all detected monoisotopic formulae and 69% of all formulae (i.e., including ^{13}C isotopologues).

2.4. Derived indices and multivariate statistical analysis

All measured intensities in the dataset were normalized to the overall spectrum intensity. Weighted mean values of the core formulae dataset were calculated for the following parameters: number of elements (#C, #H, #O), modified aromaticity AI_{mod} (Koch and Dittmar, 2006, 2016), double bond equivalent (DBE) and subsequent parameters as H/C, O/C, DBE-O. A comprehensive overview of all indices has been given in Roth et al. (2015). Information on elemental composition allows the grouping of molecular formulae into compound groups (Rossel et al., 2016). The relative contribution of each compound group was assessed in two ways, based on the relative number of molecular formulae and based on their contribution to total FT-ICRMS signal intensity.

We considered the following compound groups (modified after Šantl-Temkiv et al. (2013)): BC (polycyclic condensed aromatics, such as "black carbon"), lwBC (BC formulae < 15 C atoms), hwBC (BC formulae ≥ 15 C atoms), HU (highly unsaturated), PEP (unsaturated, oxygen and nitrogen containing compounds, such as peptides), PP (polyphenols), lwPP (PP formulae < 15 C atoms), hwPP (PP formulae ≥ 15 C atoms), SFA (saturated, O-containing, such as fatty acids), UA (unsaturated aliphatics), and SUG (very high O-content, such as sugars). This classification is based on thresholds for #C, H/C, O/C, AI_{mod} and the presence of N in the respective molecular formulae (Supplementary Table S6). It is important to point out that information on molecular formula alone provides only basic structural information; the assignment of compound groups is therefore not necessarily unambiguous (Rossel et al., 2016). All indices and compound group data (see Supplementary Tables S7–S9) were derived for each sample based on the core set of formulae.

To estimate a sample's chemical diversity in terms of formulae, we furthermore calculated the Shannon index H′ for some samples (Jost, 2006):

$$H' = -\sum_{i}^{S} p_i \times \ln(p_i)$$

With i – the ith molecular formula of S total formulae, and p_i – the abundance fraction of the ith molecular formula of the total ion abundance of that sample (ln, natural logarithm). The index can be used as a measure of predictability of a community of molecular formulae of a given DOM sample. An overview of diversity measures for DOM applications can be found in Mentges et al. (2017).

All statistical analyses were performed in RStudio (version 1.1.456, R Development Core Team, 2009) by using the packages vegan (version 2.0-10), and stats (version 3.1.1). Principal coordinates analysis (PCoA) allows the use of non-Euclidian distance measures (here, the Bray-Curtis dissimilarity) that account for the absence of formulae in the data (Ramette, 2007). Relations between environmental and derived parameters and principal coordinates were analyzed by post-ordination vector fitting methods (function envfit, 999 permutations). Linear correlations between variables and the ordination are shown as vectors. Their direction marks "most rapid change in the [...] variable", while length is "proportional to the correlation between ordination and [...] variable" (Oksanen, 2015). To find responses of specific groups of compounds in terms of systematic patterns in van Krevelen space, we correlated mixing gradients of single molecular formulae with principal coordinates and environmental variables.

3. Results

3.1. Characterization of endmembers and bulk mixing effects

In situ pH values of the river waters during the sampling campaign were slightly acidic and between 4.87 and 5.20 for the Rio

Negro and its tributaries Tarumã Mirim and Tarumã Açu (samples 8 and 18–20, Fig. 1, Table 2). The Rio Solimões endmember (sample 17) had a pH of 7.07, and all samples along the mixing transect between the Solimões and Rio Negro (samples 9–16) had pH values between 6.13 and 6.86. Electrical conductivity ranged between 8.9 μS/cm (Rio Negro) and 78.4 μS/cm (Solimões). Rio Negro samples were characterized by higher DOC concentration (in the following, given as mean and standard deviation of all three sample sets; 7.7 ± 0.4 mg C/L, Table 2, Supplementary Tables S1 and S2) than Rio Solimões samples (3.9 ± 0.5 mg C/L). Using conductivity as a water body tracer, conservative mixing of DOC was observed throughout all sample sets with only two NAT samples deviating from the trend (Fig. 2a, samples 10 and 11). These deviations coincided with high levels of elements usually related to inorganic particles (Fe, Al, Co, Ni; Supplementary Fig. S6). DOC concentrations in the smaller blackwater tributaries were in a similar range to the Rio Negro, with the exception of sample 20 (Rio Tarumã Mirim/Rio Negro confluence) which showed four times higher DOC concentration than the other tributaries (25.4 mg C/L).

Dissolved Fe concentrations were generally higher in Rio Negro endmembers (215 ± 27 μg/L) in contrast to Rio Solimões endmembers (132 ± 36 μg/L), with the exception of sample 17 (240 μg/L). About 50 μg/L of Fe was lost by filtration in both endmember samples which is about 20–30% of the total Fe (Supplementary Tables S1 and S2). Conservative mixing was only observed for Fe when particles were absent. When particles were present in the environmental samples and in the experiment, the mixing curve resembled a "sawtooth" pattern; maxima (positive anomalies of d.Fe) occurred above the conservative mixing line at mixing ratios (Solimões/Rio Negro) of 0.1 and 0.8 and values below the conservative mixing line (negative anomaly of d.Fe) between ratios of 0.4–0.7.

Rio Negro endmember samples were characterized by a lower Cu content (0.5 ± 0.3 μg/L) compared to the Rio Solimões endmembers (2.3 ± 1.2 μg/L). As with Fe, the mixing behavior of Cu was conservative in the experiment with filtered river endmembers. In the non-filtered samples (MIX NF) Cu also behaved conservatively up to a mixing ratio of 0.5 but there were significantly increased Cu concentrations in the mixing range 0.6–0.8, indicating a release of Cu from particulate matter under the influence of Rio Negro water (Fig. 2c, Table 2, Supplementary Tables S1). Interestingly, in the set of natural samples all Cu values along the mixing transect were higher than in the experiment. Cu levels were notably elevated in the NAT endmembers (Solimões, No. 17: 5.4 μg/L; Negro, No. 8, 5.9 μg/L), largely deviating from the rest of the samples in the mixing zone. The TDCu data from CLE-AdCSV indicated much lower values (Table 2) for these samples.

Aside from significant differences, which will be presented below, the river samples were overall highly similar in their molecular composition (Fig. 3). Based on all detected monoisotopic formulae along the three mixing gradients (n = 3982), the sample sets shared 88% of their formulae (n = 3478). Sample set-specific similarity in molecular composition among both endmembers, as determined by the Jaccard index (*J* [%] = number of common formulae divided by number of common formulae + sample-specific formulae), was 85% (MIX NF), 81% (MIX F) and 79% (NAT). NAT endmembers were thus the most dissimilar. Related Bray-Curtis dissimilarities (*BC* [%] = sum of intensity difference divided by intensity sum) were 13% (MIX NF), 15% (MIX F), and 18% (NAT). *J* and *BC* do not add up to 100% similarity here because the indices are based on different data (numbers vs intensities of shared and all formulae).

For comparison, repeated measurements (n = 4) of a PPL extract of a eutrophic lake sample yielded similarity values of 96.6 ± 0.3% and dissimilarity values of 2.3 ± 0.4%. The overall similarity of the endmembers was also evident from a similarly high molecular diversity as determined by the Shannon Index (MIX NF Negro, Hs = 7.65; MIX NF Solimões, Hs = 7.61) and similar extraction efficiencies (see Section 2.2).

For further investigations, only common formulae ("core data set") detected in both MIX sample sets were analyzed, reducing the allover formula number to n = 3608 (90% of all monoisotopic formulae). Even though site-specific molecular formulae are not considered in this approach, clear differences in FT-ICRMS signal intensities are still preserved on an individual molecular formula level (Zark and Dittmar, 2018). The 374 excluded formulae showed no consistent mixing patterns of removal or release. Regardless of the high similarity in endmember's molecular composition, i.e. presence of similar formulae, Rio Negro samples were characterized by higher abundance of aromatic constituents (PP, BC) and lower abundances of unsaturated aliphatic (UA) and highly unsaturated (HU) compounds (significant differences, Student's *t*-test, Supplementary Table S10).

On average, molecular formulae in the Rio Negro samples contained more C and O, and less H, and consequently showed higher average molecular mass (*m*/*z*), higher O/C, higher AI_{mod}, and higher DBE and lower H/C. For example, the mean (weighted average) monoisotopic atom abundance for the Rio Solimões (across all sample sets, not including technical replicates) was $^{12}C_{18.2\pm0.3}$, $^{1}H_{21.9\pm0.3}$, $^{16}O_{6.4\pm0.04}$, $^{14}N_{0.11\pm0.01}$, $^{32}S_{0.052\pm0.005}$ and $^{31}P_{0.005\pm0.001}$, while it was $^{12}C_{18.4\pm0.2}$, $^{1}H_{21.1\pm0.2}$, $^{16}O_{6.9\pm0.2}$, $^{14}N_{0.08\pm0.01}$, $^{32}S_{0.041\pm0.005}$ and $^{31}P_{0.006\pm0.001}$ for Rio Negro.

Differences in mass spectra included a higher abundance of signals in the range of 150–250 Da in Rio Negro samples, as compared to their Solimões counterparts that showed marked increase of abundance distribution in the range of 250–300 Da (Fig. 3). Subgrouping of the molecular formulae into compound groups supported this finding by revealing the contribution of small, hydrogen-deficient formulae to the lower mass region in the Rio Negro samples (Fig. 4, Supplementary Table S10, lwPP, lwBC), reflecting the overall higher aromaticity of these samples.

Small condensed polycyclic aromatics were preferentially enriched in blackwater samples that drain large areas covered by rainforest vegetation and sandy soils. These compounds have a low molecular mass (lwBC) and contain three or fewer aromatic rings (threshold of 15C atoms). In addition, aromatic compounds were also significantly elevated above 250 Da (Supplementary Table S10; hwPP, hwBC). Compounds classified as highly unsaturated (HU) or unsaturated aliphatic (UA) compounds were assigned over the whole mass range but were generally elevated in the Solimões endmembers. The molecular groups of highly oxygenated compounds, such as sugars (SUG), saturated fatty acids (SFA) and unsaturated nitrogen-containing peptide-like compounds (PEP) were of lower abundance in terms of formula number and intensity.

3.2. Local variability in DOM molecular composition and mixing dynamics in the initial confluence

The local tributary samples from Rio Tarumã Mirim and Rio Tarumã Açu showed separation from Rio Negro (NAT 08) and Rio Solimões (NAT 17) samples by principal coordinates analysis (PCoA, Supplementary Figs. S8 and S9). Notably, sample 20 from the tributary's mouth clustered with the other blackwater tributary samples and had a DOC content that was four times higher. Three spatially proximate samples of the NAT set (09, 11 and 12, Fig. 1) stood out in their DOM molecular composition, showing a strong similarity in their DOM characteristics (Supplementary Fig. S8b) as opposed to the other samples and the conservative mixing line. The three samples were included into the analysis of all local samples (including endmembers from all samples sets, and local tributary samples) due to their deviating DOM properties

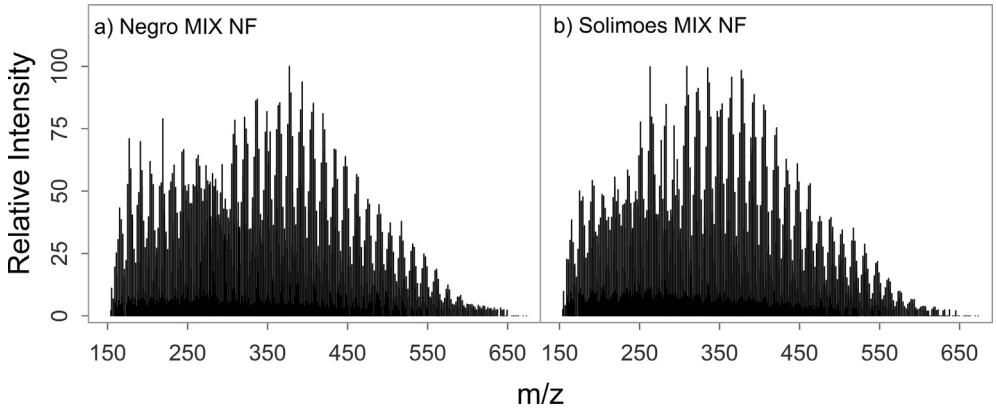

Fig. 3. FT-ICR mass spectra of: (a) Rio Negro and (b) Rio Solimões (both MIX NF set, only assigned molecular formulae shown) are mainly discerned by signals in the lower mass range below 350 Da. This is preserved after filtration (MIX F) and also found in river samples from August 2013 (NAT sample set).

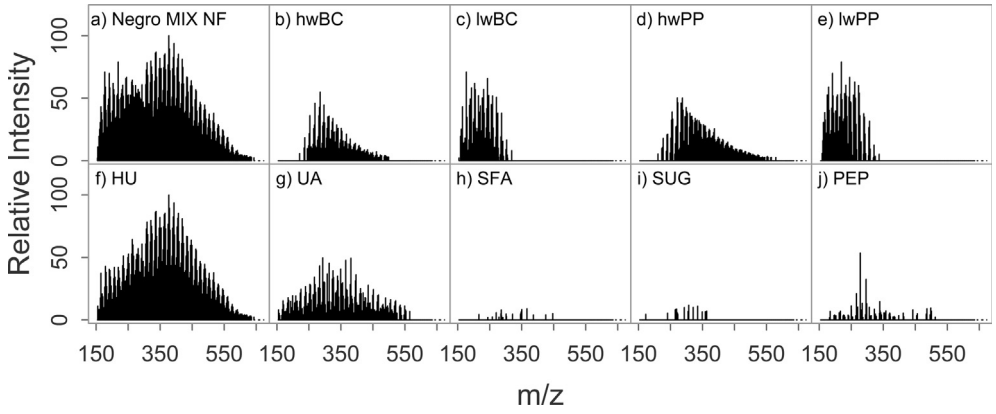

Fig. 4. (a) Rio Negro FT-ICR mass spectrum (same as Fig. 3a) separation according to molecular groups reveals distinct distribution patterns found across all sample sets (b, c: black carbon, BC; d, e: polyphenols, PP; < 15 C atoms, "lw"; ≥ 15 C atoms, "hw"; f: "highly unsaturated", HU; g: unsaturated aliphatics, UA; h: saturated fatty acids, SFA; i: sugar-like, SUG; j: peptide-like, PEP; see also Supplementary Materials Section 3). Hydrogen-deficient formulae and small ("lw") BC- and PP-like formulae strongly contribute to the lower mass region indicative of a Rio Negro influence.

but excluded from the mixing gradient analysis (see reasoning in Supplementary Note S4).

Sample NAT 09, even though sampled in Rio Solimões water and showing high conductivity, showed similar features to the Rio Negro sample (NAT 08). Samples 11 and 12 displayed extraordinarily high weighted mean values of molecular mass (m/z), number of C and O atoms, DBE and O/C (Supplementary Table S7).

PCoA separated Rio Negro and Rio Solimões in a similar fashion (Fig. 4a and b), with clear differences between sampling dates (2013 vs 2014). Filtration effects were apparent but relatively small compared to the overall variability. Based on subtraction of normalized mass spectra, differences between samples mostly arose from individual formulae of low intensity and were most pronounced for the PEP molecular group (Supplementary Note S5). Post-ordination fitting of spectral indices (e.g., maximum intensity), derived indices (e.g., weighted average of DBE) and environmental variables (concentrations of DOC, Cu and Fe) revealed potential links to "synthetic" gradients, i.e. calculated ordination coordinates, of molecular compositional change. The first coordinate was related to mass shift and degree of oxygenation (positive: DBE-O, SUG, SFA; negative: m/z, #O, O/C, HU), whereas unsaturation-related changes and DOC concentration were related to the second (positive: DBE, #C, AI_{mod}, PP, BC; negative: H/C, #H, UA, PEP) and third coordinate (positive: DOC; neg: I_{max}). Both the DBE and AI_{mod} were lower in Rio Negro and Rio Solimões samples taken in October 2013 (NAT) as compared to samples taken in August 2014 (MIX). Consequently, compounds classified as BC contributed less to their compound pool. The group of unsaturated aliphatic compounds (UA) showed a markedly higher contribution in the 2013 samples (NAT) in both endmembers leading to an overall elevated H/C ratio (Supplementary Table S10).

3.3. Statistical analyses of molecular-level DOM mixing dynamics

The statistical analyses employed here were conducted in three steps. To assess major variation in DOM, we first performed PCoA. Thereafter, we linked the coordinates to gradients of environmental variables and DOM molecular indices, and finally analyzed correlation patterns of those variables in van Krevelen space.

Sample set-specific PCoAs (step 1 of the analysis) indicated the presence of a dominant gradient in all sets (Fig. 5). The first coordinate held a large part of the total variation (56–65%), while the second and third coordinates accounted for <20% (Figs. 6 and 7, Supplementary Figs. S8 and S9). The dominance of the first coordinate was highest in the particle-free mix (MIX F). In turn, the fraction of variation explained by the second and third coordinates was lowest for this dataset (8% and 5%, respectively). In accordance with the bulk DOC concentrations, the mixing ratio of both endmembers was the main controlling factor of the molecular composition and highly linked to the first coordinate in all datasets

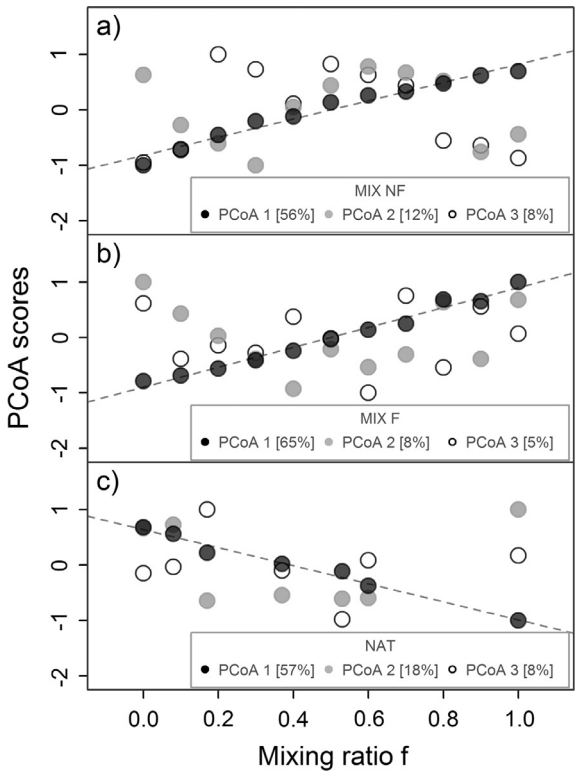

Fig. 5. PCoA scores of the first three coordinates of all three experiments: (a) MIX NF, (b) MIX F, and (c) NAT, plotted against the mixing gradient f. Coordinate 1 is always strongly correlated with the mixing gradient. By definition the remaining coordinates are independent of the first coordinate and thus carry the main non-conservative variability within all DOM datasets; explained variability is shown in percent in the legends.

(mixing ratio f, Figs. 5, 6a and 7a, Supplementary Fig. S10). The lower order coordinates thus enabled us to extract the main gradients (Figs. 6 and 7) of remaining (non-conservative) variability independent from the main variation caused by (conservative) mixing.

In a second step, we linked external and internal controls on DOM variability with principal coordinates. Spectral and chemical indices – either derived directly from the mass spectra (i.e., weighted mean of molecular mass (m/z)) or from the molecular formula data (i.e., DBE) – were mainly correlated ($p < 0.05$, $n = 11$) to the dominant first coordinate. These variables thus exerted a high redundancy to the effect of mixing, as expected from the results of the PCoA separation (Fig. 6a). Similar trends were presented for MIX F (Fig. 7a) and, with single exceptions, also for NAT sample sets (Supplementary Fig. S10).

The molecular group data (Fig. 6) showed a differential response in MIX NF, indicating non-conservative effects. Several molecular groups correlated with coordinate 2 (PCoA 2) in the MIX NF ordination (Fig. 6b and c), while these variables were mainly linked to simple mixing (correlated to coordinate 1 (PCoA 1)) under absence of particles (MIX F, Fig. 7b and c). This encompassed the groups of aromatic compounds (PP and BC) and unsaturated, nitrogen-containing compounds (PEP).

The non-conservative fraction of Cu (d.Cu, $p = 0.036$, $R^2 = 0.58$) showed a similar correlation with coordinate 2 in the MIX NF ordination and was a marked exception to the general trend of environmental variables being controlled by mixing in both MIX datasets (Figs. 6d and 7d). The aromatic PP and BC molecular groups were positively related to Cu release (all groups, $p < 0.01$ based on relative number or intensity). Interestingly, the PEP group and the d.PEP (designating the non-conservative fraction of relative PEP abundance, similar to the described d.Cu value) correlated to the second coordinate in both MIX NF ($p = 0.003$; $R^2 = 0.91$) and MIX F ($p = 0.018$, $R^2 = 0.65$), in particular to changes in PEP signal intensity (Fig. 6c). Changes in the relative intensity of PEP compounds thus indicated a similar non-conservative response in both MIX experiments independent of the presence of particles. In contrast, we only found a significant correlation of changes in the number of PEP compounds when particles were present (MIX NF, $p = 0.001$, $R^2 = 0.91$), but not in absence of particles (MIX F, $p = 0.075$, $R^2 = 0.49$, Fig. 7b). In turn, we only found a negative correlation between the number of PEP compounds and Cu release when particles were present.

In a third step, we searched for indicative patterns in van Krevelen diagrams to reveal chemical properties of formulae driving the variability (Figs. 8 and 9, Supplementary Fig. S11). The correlation of mixing gradients of single molecular formulae with synthetic (principal coordinates) and environmental variables (f, d.Cu) revealed distinct differences in number of responding formulae but also clear correlation patterns in van Krevelen space (Figs. 8 and 9; Pearson's r, see Supplementary Fig. S12 for details of the correlation analysis). A large proportion of formulae fluctuated in FT-ICRMS signal intensity during mixing but did not show consistent non-conservative behavior (Supplementary Figs. S13 and S14, and Supplementary Note S6).

Formulae in the region of hydrogen-deficient (aromatic-type) compounds were positively correlated (all correlations, $p < 0.05$) to the first coordinate and thus to the mixing gradient f, while a broad fraction of more hydrogenated (less aromatic) formulae was negatively correlated to it (Figs. 8a and 9a). We found the same trend for the NAT set (Supplementary Figs. S10 and S11). The amount of formulae that significantly correlated with coordinate 1 ($p < 0.05$) were highest for MIX F ($n = 1867$, 52% of formulae within the core dataset) and lower for sample sets MIX NF ($n = 1576$, 44%) and NAT ($n = 976$, 27%). Thus, in the case of MIX F, most formulae were significantly correlated with the conservative mixing gradient, and the distribution of negatively correlated formulae included higher H/C ratios (greater contribution from saturated and PEP compounds). Due to the strong correlation between mixing gradient f and coordinate 1 in all experiments, their van Krevelen correlation patterns were highly similar (Figs. 8c, 9c and Supplementary Fig. S11c).

The second coordinate correlated with a variety of evenly distributed formulae except for a cluster in the region of saturated and PEP compounds (Fig. 8b and 9b). The number of correlated formulae was about 4% for both MIX sets, but the amount of correlated formulae in the PEP region was higher in MIX NF. The second coordinate correlation pattern of the NAT sample set was highly different from the MIX set patterns (Supplementary Fig. S11). Regarding MIX NF, the behavior of the metals Fe and Cu was reflected by similar correlation patterns (Fe not shown). Additionally, the correlation patterns of PCoA 2 and d.Cu showed a high similarity, especially regarding the negatively correlated PEP cluster (Fig. 8d). In case of Fe, no such distinct regions of the plot could be connected to its non-conservative behavior.

4. Discussion

4.1. Properties of endmembers

The endmember concentrations of DOC, Fe and Cu were in ranges reported in the literature (Aucour et al., 2003; Gaillardet et al., 2014; Mulholland et al., 2015). Blackwater samples stood out in their DOM molecular composition due to their higher aromaticity (Figs. 3, 4 and 6–9). Interestingly, this was in part caused

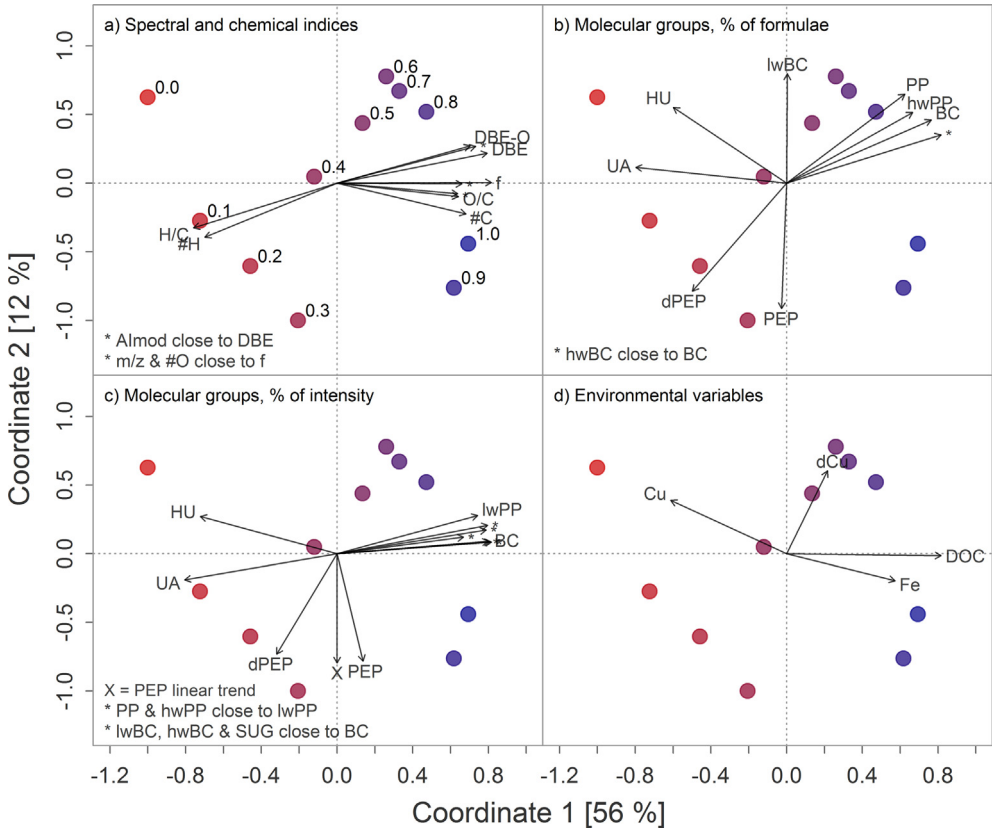

Fig. 6. MIX NF ordination plots with four different sets of added variables (post-ordination gradient fit, a–d), f values given in (a). MIX NF samples are separated by a dominant first coordinate linked to the mixing ratio, along with most chemical indices based on molecular formula data (panel a). The second coordinate represents the major part of non-conservative variation in molecular composition and is mainly linked to variables in panels b–d. Colors refer to the mixing gradient, blue being the Rio Negro endmember. Significant correlations (Pearson, $p < 0.05$) with the ordination are shown as arrows. Arrow length corresponds to strength of correlation and arrows head into the direction of steepest increase of the respective variable, based on the ordination pattern of samples. Variable abbreviations: AI_{mod} (modified Aromaticity Index), BC ("black carbon"), lwBC (BC formulae < 15 C atoms), hwBC (BC formulae ≥ 15 C atoms), d.Cu (non-conservative fraction of dissolved Copper), DBE, DBE-O (double bond equivalents, DBE minus oxygen), f (mixing ratio), H/C ratio, HU (highly unsaturated), *m/z* (molecular weight, mass to charge ratio), O/C ratio, PEP (unsaturated, O- and N-containing), d.PEP (non-conservative fraction of peptides), PP (polyphenols), lwPP (PP formulae < 15 C atoms), hwPP (PP formulae ≥ 15 C atoms) SFA (saturated, O-containing), UA (unsaturated aliphatics). (For interpretation of the references to color in this figure legend, the reader is referred to the web version of this article.)

by elevated abundances of aromatic compounds in the mass range <250 Da (Figs. 3 and 4). The overall higher aromaticity of Rio Negro samples has been described by Ertel et al. (1986) who extracted humic (HA) and fulvic acids (FA) on hydrophobic resin (XAD-8), assigning ~70% of both HA and FA fluxes at the confluence to Rio Negro inputs. Rio Negro HA and FA were reported to be more degraded than similar HA and FA isolates from other blackwater or whitewater tributaries (based on lignin compositional changes), in conjunction with a lower H/C ratio.

Biodegradation might explain the strong contribution of small molecules, but recent findings suggest that contributions of low-molecular weight constituents in FT-ICRMS data may be related to "fresh" or freshly decomposing material (Roth et al., 2016). Compounds belonging to the lwBC class are not necessarily combustion-derived, but a biogenic source cannot strictly be excluded. The preferential occurrence in blackwater samples may suggest a link to leached plant metabolites or products of plant litter breakdown. Low retention of organic matter in bleached soils of the Negro basin (arenosols, podzols; Fritsch et al., 2009; Bardy et al., 2011; Quesada et al., 2011) could explain apparently fresher and more aromatic riverine DOM in blackwater catchments.

Aromatic structures also contributed to a distinct Rio Negro signal in the higher mass range in our study (Supplementary Table S10), paralleling shifts in elevated oxygen and carbon content (see Section 3.1) which could point to larger, more oxidized structures. Specific larger structures have been described for Rio Negro DOM (Gonsior et al., 2016). Recent findings by Waggoner and coworkers suggest molecular mechanisms that could explain strong degradation as observed by Ertel et al. (1986) and high molecular weight as observed by Gonsior et al. (2016) and Johannsson et al. (2016). Waggoner et al. (2015) reported on the abiotic transformation of a lignin extract from a brown rot fungal degraded wood sample by hydroxyl radical (·OH) action, and present evidence for the formation of condensed, higher-weight aromatic structures from the initial lignin extract. Subsequent fractionation of the extract before ·OH exposure indicated that the most polar fraction of the lignin mixture contributed largely to this shift, in terms of formula number (1673–2437; treated vs untreated), as well as magnitude-weighted mass (average *m/z;* 490–574) and aromaticity index (0.31–0.52, Waggoner and Hatcher, 2017). Photochemical reactions and fungal enzymes contribute to the formation of hydroxyl radicals in water bodies and soils and can potentially alter DOM signatures in this way (Waggoner et al., 2015; Johannsson et al., 2016; Waggoner and Hatcher, 2017).

In contrast, a stronger contribution of smaller and moderately unsaturated to saturated (HU, UA) compounds in Rio Solimões endmembers (Figs. 8a, 8c, 9a and 9c) may reflect former particle-bound OM in streams rich in suspended sediments. Suspended particles from whitewater Amazonian rivers can be enriched in nitrogenous compounds (Aufdenkampe et al., 2001) and may transport more sorbed organic compounds in general (Kleber

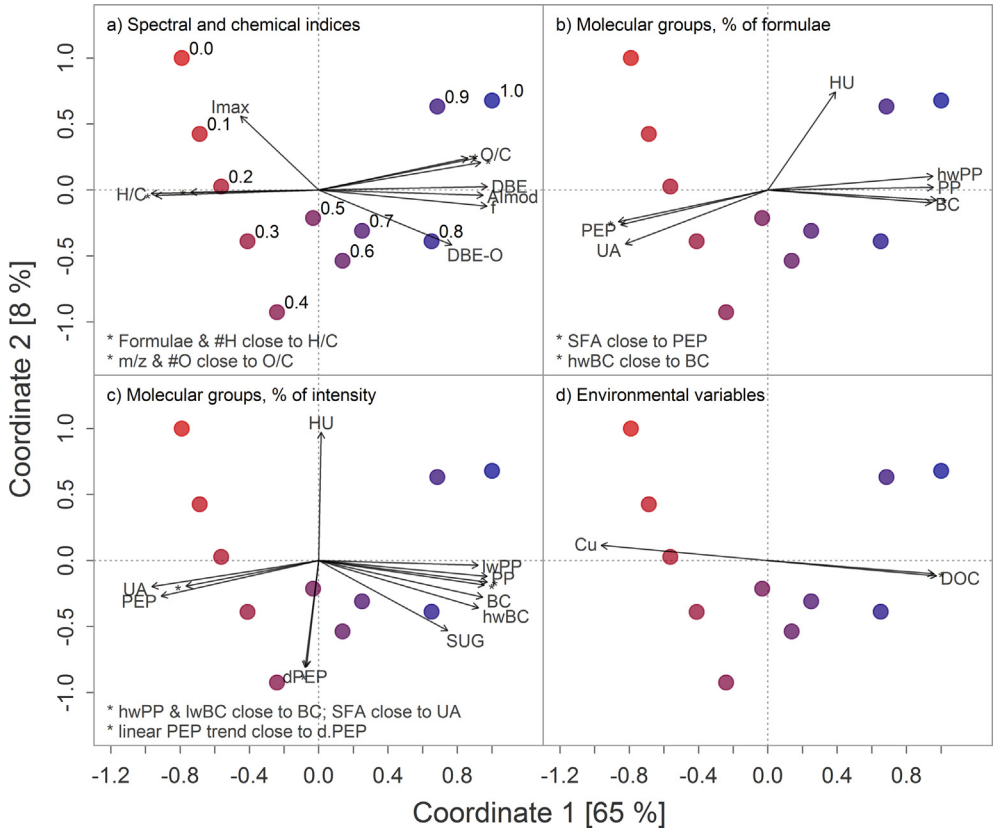

Fig. 7. MIX F ordination plots with four different sets of added variables (post-ordination gradient fit, a–d); f values given in (a). The absence of particles causes differences in the variable's links to the ordination as compared to Fig. 6. For MIX F, the degree of explained variance by the first coordinate is even higher than for MIX NF (Fig. 6). The second coordinate represents the largest part of non-conservative variation in molecular composition, but less of the analyzed variables are connected to it. Significant correlations (Pearson, $p < 0.05$) with the ordination are shown as arrows. Arrow length corresponds to strength of correlation and arrows head into the direction of steepest increase of the respective variable, based on the ordination pattern of samples. Variable abbreviations: AI_{mod} (modified Aromaticity index), BC ("Black Carbon"), lwBC (BC formulae < 15 C atoms), hwBC (BC formulae ≥ 15 C atoms), d.Cu (non-conservative fraction of dissolved Copper), DBE, DBE-O (double bond equivalents, DBE minus oxygen), f (mixing ratio), Imax (maximal rel. intensity), H/C ratio, HU (highly unsaturated), *m/z* (molecular weight, mass to charge-ratio), O/C ratio, PEP (unsaturated, O- and N-containing), d.PEP (non-conservative fraction of peptides), PP (polyphenols), lwPP (PP formulae < 15 C atoms), hwPP (PP formulae ≥ 15 C atoms) SFA (saturated, O-containing), UA (unsaturated aliphatics).

et al., 2007), as opposed to the low amount of suspended sediment carried by the Rio Negro. Moreover, >90% of the sediment load of the Rio Negro is composed of kaolinite clay minerals with low adsorption capacity (Irion, 1991).

The two groups of endmember-related formulae (Rio Negro/Rio Solimões) showed distinct characteristics, including H/C ratio, aromaticity, *m/z* range and intensity distribution as opposed to the remainder of non-correlated formulae (Supplementary Figs. S15–S18), indicating not only differences in unsaturation but also molecular weight range and abundance of river-specific signals being in line with previous reports (Gonsior et al., 2016).

It is intriguing that the aromaticity of DOM is elevated when water levels of both rivers have peaked and are starting to decrease again (Supplementary Fig. S1, July 2014, as opposed to samples from October 2013), and that N-containing formulae seem to be more prominent at the onset of the flood peak, at least in Rio Negro waters (i.e., when water levels are rising; Gonsior et al., 2016; see further discussion in Section 4.3). These time points correspond to maximum and minimum levels of the hydrograph, respectively, indicating a watershed-scale time lag of inputs vs outputs via precipitation and river channels (Supplementary Fig. S1). Although the differences in DOM composition may indicate seasonal differences related to stronger flushing of soils (as a potential source of aromatic DOM, as discussed above), hydrological pulse/flooding of wetlands, or internal processing of organic matter (also in light of other data from May 2016; Gonsior et al., 2016, see Section 4.3), one has to point out that endmembers showed a surprisingly large similarity in our study (Section 3.1). Given the small temporal resolution of our study and reported data, it is evident that further work is needed to resolve potential river-specific DOM composition changes driven by seasonality or watershed properties.

4.2. General trends during mixing

The DOC concentrations showed two local maxima and besides that generally a linear trend in the NAT sample set, which was consistent with conservative mixing observed in MIX experiments (Fig. 2a). We found no evidence for a consistent DOC anomaly (i.e., removal or release of DOC) in all experiments. The two deviating NAT samples indicated a DOC release at separate mixing ratios (open circles at f = 0.9 and 0.53, Fig. 2a), which may rather be explained by natural variability than by consistent non-conservative effects. Furthermore, the mixing curves of concentrations of Fe (Fig. 2b) and other particle-associated elements (Al, Co, Ni; Supplementary Fig. S6) showed coinciding maxima in concentration at these mixing gradient positions. Interpretation of the underlying effects is difficult without further information on the concentration and nature of particles (as, for example presented by Guinoiseau et al., 2018). A strong removal of Cu from solution was detected at low Rio Negro concentrations (Fig. 2, f < 0.4). This might imply a fast removal of colloidal Cu transported by the Solimões upon mixing with DOC-rich waters of the Rio Negro. The

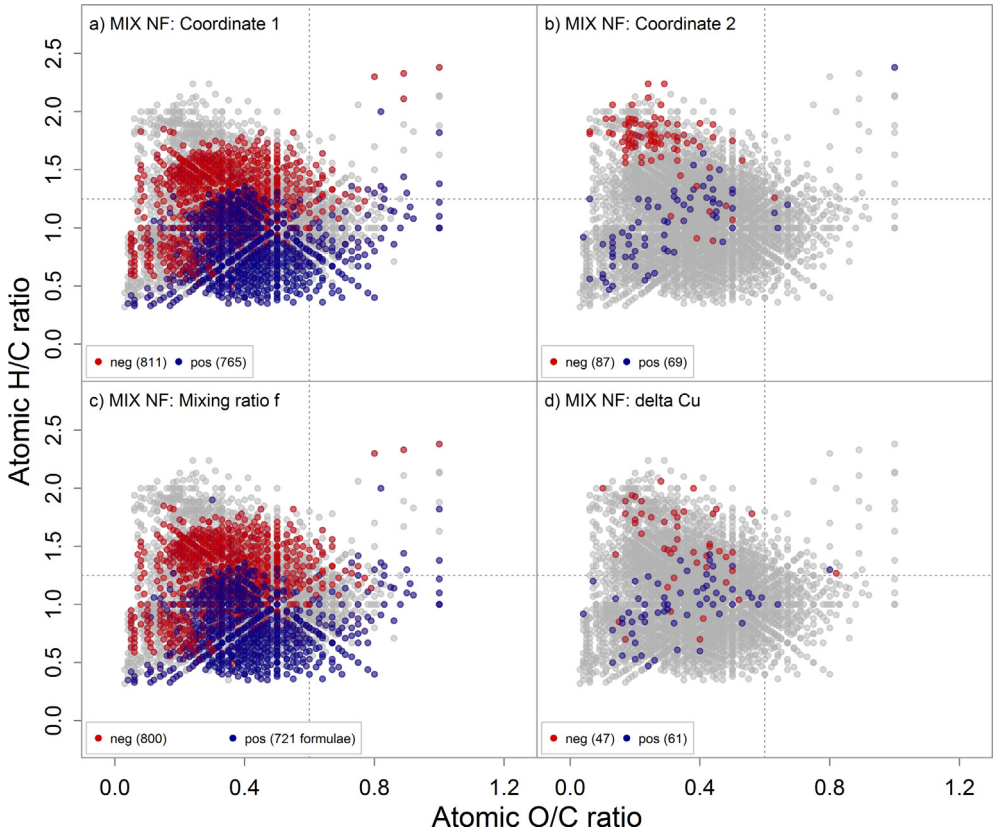

Fig. 8. Van Krevelen plots of correlations with (a) principal coordinate 1, (b) principal coordinate 2, (c) mixing ratio f and (d) d.Cu (non-conservative fraction of dissolved Copper), shown for the MIX NF sample set. Numbers in the legend refer to the number of either positively or negatively correlated formulae. Only significant correlations (Pearson, $p < 0.05$) are shown in color, non-significant formulae are gray. A large number of formulae mix conservatively, with Rio Negro-linked signals being concentrated in the less saturated (~more aromatic) region of the VK plot.

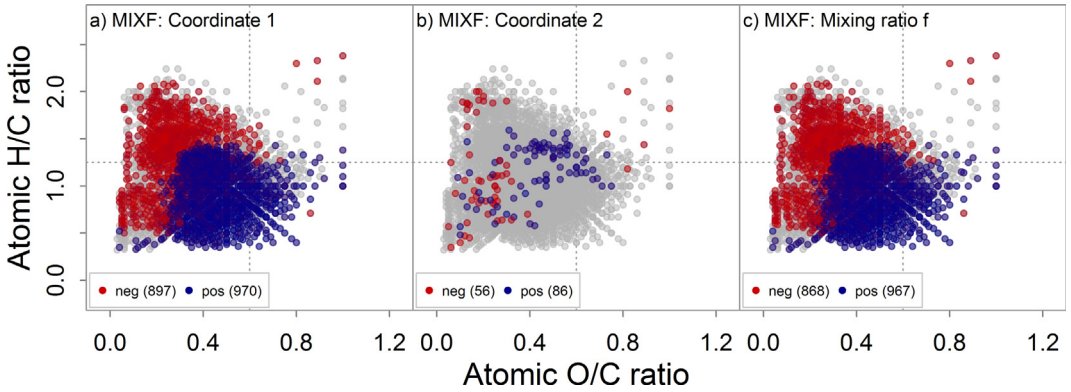

Fig. 9. Van Krevelen plots of correlations with (a) principal coordinate 1, (b) principal coordinate 2 and (c) mixing ratio f, shown for the MIX F sample set. Only significant correlations (Pearson, $p < 0.05$) are shown in color, non-significant formulae are grey. Numbers in the legend refer to the number of either positively or negatively correlated formulae. A number of formulae in the saturated region of the VK plot (upper red cluster in panel b) show non-conservative behavior even when particles are absent. (For interpretation of the references to color in this figure legend, the reader is referred to the web version of this article.)

strong removal of Cu might be concentration-dependent as it was not detected in the MIX NF experiment, but this could also be related to differences in particle concentration during both sampling campaigns.

Samples 08 and 17 showed very high Cu concentrations as determined by ICPMS (>5 μg Cu/L) whereas the TDCu levels determined by CLE-AdCSV were much lower (0.73 and 2.99 μg Cu/L, Table 2). Endmember sampling differed from the other NAT samples in that more volume and different flasks were taken (for other measurements; Merschel et al., 2017), which could explain this contrast. We considered TDCu data more reliable due to the shorter storage before measurement and similar handling of the respective subsamples. ICPMS and CLE-AdCSV indicated similar dissolved Cu concentrations in samples 10 and 15, while the TDCu concentration was slightly elevated in sample 12 (determined by CLE-AdCSV).

Fe concentrations of field samples from the mixing zone were in the same range and showed similar dynamics as observed in the

MIX NF experiment. Strong variation ("sawtooth" patterns) in Fe concentration during mixing are described in the literature and have also been observed during mixing experiments with river water and seawater for Ti and Zr (Schneider et al., 2016). Such behavior may be related to the dynamics of particles or surface phenomena and has also been linked to differential behavior of distinct Fe pools, as colloidal and dissolved Fe (Aucour et al., 2003; Gaillardet et al., 2014; Mulholland et al., 2015). Higher concentrations of Cu in samples of the NAT set (as opposed to the MIX set) could be explained by interannual variability, even though Cu concentrations were similar to values previously reported by Küchler et al. (1994) and Viers et al. (2005). Seasonality patterns and interannual variability of Cu and other elements have been described by several authors (Viers et al., 2005; Gaillardet et al., 2014). Fe and Cu behavior will be further discussed within the context of DOM dynamics (Section 4.4).

Multivariate analyses of the MIX and NAT sample sets showed a dominant first coordinate with 56–65% of variation, which was correlated to the mixing gradient and several molecular characteristics of DOM (Figs. 6 and 7; inversely correlated to f in NAT, Supplementary Fig. S10). Samples 11 and 12 exhibited a higher mean mass, a higher DBE and contained on average more carbon and oxygen than other NAT samples. Sample 9, although taken in Solimões waters, resembled the Rio Negro endmember (8), and thus also samples 11 and 12, in many properties. This does not necessarily indicate non-conservative effects. The similarity of these three samples (Supplementary Fig. S8) and their spatial proximity (Fig. 1) rather suggest a common source. It is thus concluded that these samples might have been influenced by a third (unsampled) interfering endmember, possibly from draining floodplains (Viers et al., 2005; Supplementary Fig. S8, Supplementary Note S4). After removal of the three deviating samples, the multivariate analysis agreed well with results obtained in the mixing experiments in the presence of particles (MIX NF). In summary, we observed: (1) conservative behavior of DOC and DOM-derived parameters, and (2) non-conservative behavior of Cu and Fe, which will be discussed in detail in Sections 4.3 (conservative component) and 4.4 (non-conservative component).

Multivariate statistics revealed a high variation of DOM molecular composition in the natural confluence as compared to the sole effect of a two-endmember-mixing process (Supplementary Figs. S8 and S9a). The strong variation on a relatively small temporal and spatial scale was an unexpected result of our study. To reduce the influence of natural variability in studying mixing effects and processes, we performed controlled mixing experiments with defined endmembers.

4.3. The conservative component of mixing

Unexpectedly, the concentration of DOC displayed conservative mixing in NAT and MIX experiments with only few exceptions (Fig. 2a). This is a surprising finding, since DOC is generally described as reactive in the confluence zone of Negro and Solimões (Table 1). Several studies have confirmed losses and fractionation of DOC in the initial mixing (Ertel et al., 1986; Aucour et al., 2003; Moreira-Turcq et al., 2003a), although there is evidence for simple dilution by mixing (Moreira-Turcq et al., 2003a). Mulholland et al. (2015) showed that dissolved Fe (<0.45 μm) behaved conservatively during initial mixing, whereas dissolved and colloidal Fe started to behave non-conservatively 1–10 km after mixing in the river. The study also reported a high degree of organic Fe complexation. Their results suggest that the conservative behavior of DOC concentration under conditions of the natural confluence (NAT) might be due to small contact times of particles and DOC (i.e., kinetic limits). However, our simulated mixing experiments were conducted for ~24 h, and kinetic hindrance should thus not be a critical point in explaining DOC concentration dynamics (Stedmon and Markager, 2003; Merschel et al., 2017). Moreover, there is evidence for fast sorption of Amazon DOM onto mineral phases (Aufdenkampe et al., 2001; Pérez et al., 2011). A recent study by Merschel et al. (2017) found similarly conservative behavior of DOC in mixing experiments of seawater with riverine samples from Rio Negro and Rio Solimões, concluding that much of the "dissolved" DOC in riverine samples that passes submicron filters (0.2 μm, as used in this study) may be present as organic nanoparticulate or colloidal matter, which does not readily coagulate to form larger aggregates during mixing.

The van Krevelen analysis and post-ordination gradient fitting of the mixing experiments revealed that specific fractions of the DOM compound pool were strongly linked to conservative mixing (f), and thus, to the bulk DOC concentration (Figs. 2a, 8 and 9). This fraction ranged from 27% of all monoisotopic formulae in NAT to 44% and 52% in MIX NF and MIX F, respectively. Thus, 8% more molecular formulae behaved conservatively when particles were absent in the MIX experiments. The molecular properties of the molecular formulae indicative of Rio Negro and Rio Solimões have been discussed in Section 3.1. An additional analysis of the non-correlated molecular formulae (no significant correlation with f, $p > 0.05$) indicated that an additional 16% (NAT), 22% (MIX F) and 27% (MIX NF, all percentages based on the core set) showed fluctuations but no consistent non-conservative behavior (Supplementary Figs. S13 and S14, and Supplemental Note S6). Only a small number of molecular formulae correlated with coordinates 2 and 3, which held the major part of non-conservative variation in all experiments (Fig. 5, see Section 4.4).

As indicated above, the largely conservative DOC behavior is supported by artificial sorption experiments conducted by Pérez et al. (2011). The authors found that the hydrophobic fraction (sorbed to XAD-8 resin, "HPO" fraction) of Rio Negro DOC, besides sorption of ~80% of DOC (initial ca. 18 mg C/L) to fresh synthetic goethite, was not fractionated in terms of aromaticity during the process, even under large excess of DOC. Contrastingly, the aromaticity of the relatively hydrophilic fraction (XAD-8 effluent sorbed onto XAD-4 resin, "transphilic", "TPH" fraction) decreased upon sorption. Similar high levels of DOC were sorbed. Altogether, this indicated a preferential sorption of relatively hydrophilic aromatic compounds onto sediment at high DOC loads. A second sorption experiment with an isolated OM fraction from the Amazon–Curuai floodplain and organic-free natural sediment from the Curuai Várzea Lake showed much lower sorption (5–20% DOC), however, initial DOC levels were also lower in these experiments (ca. 4.2 mg C/L). The authors did not observe any fractionation in terms of aromaticity in these second experiments either. Under the natural confluence settings, with DOC concentrations in the range of the second experiment and mineral surfaces in Rio Solimões already conditioned with organic matter, sorption or fractionation of new DOM (i.e., Rio Negro DOM) may be even further reduced.

Assuming that Rio Solimões DOM and minerals were in equilibrium before mixing with the Rio Negro, occupation of sorption sites at minerals could thus explain the conservative behavior of DOC in our observations. The Solimões mainstem has three additional upstream tributaries (Rios Jutaí, Juruá and Purús) that have been classified as DOC-rich (ranging from 5.8 to 10.8 mg C/L) by Ertel et al. (1986) and thus could contribute to saturation of reactive mineral surfaces. Similarly, a white-water tributary, the Rio Branco, enters the Rio Negro ~200 km before the Amazon junction and flocculation processes involving humic substances have been reported from this upstream confluence (Leenheer and Menezes Santos, 1980). This could also explain why the investigated rivers appear so similar in their molecular composition (even without limiting the data to a conservative set of core formulae, Section 2.3), contrasting previous results from major rivers of the Amazon basin

(Gonsior et al., 2016). The fact that a majority of the indicative aromatic compounds were already part of the DOM of the Rio Solimões (and vice versa for the low-molecular weight unsaturated Solimões compounds) may document the influence of other blackwater, whitewater and floodplain systems in the draining basins of both rivers, but could also point to similar processing in both river systems that lead to similar forms of DOM residues.

It has been proposed that two DOC fractionation steps involving minerals occur in the Amazon system: one in the soils and another one in the rivers, referred to as the "regional chromatography" hypothesis (Ertel et al., 1986; Devol and Hedges, 2001; Shen et al., 2015). According to the hypothesis, the majority of reactive components within the DOC pool are effectively removed before reaching higher-order confluences such as the one in Manaus. The process could also lead to occupancy of sorption sites at minerals, rendering both educts (minerals and DOM) non-reactive (in line with findings by Pérez et al. (2011)). Although it seems yet unclear what stage (soils, rivers, or confluences) is most important in DOC removal, several studies have shown that conservative DOC behavior in aquatic settings (riverine and estuarine) may be more frequent than previously expected (Laane, 1980; Mantoura and Woodward, 1983; Palmer et al., 2015; Ylöstalo et al., 2016; Merschel et al., 2017).

Non-conservative effects may be rare and subtle in space (Guinoiseau et al., 2016) or time (Palmer et al., 2015), similar to observations from terrestrial systems (Kuzyakov and Blagodatskaya, 2015). More than 80% of river length of the Amazon River system is connected to the smallest streams (first and second order streams; McClain and Elsenbeer, 2001). It seems certain that the role of these smaller tributaries and lower order confluences will be underestimated when only large confluences are considered; non-conservative processes might already have taken place further upstream or even directly at the soil/water interface (Guinoiseau et al., 2017; Ward et al., 2017).

Gonsior et al. (2016) found strong dissimilarities of DOM molecular composition between rivers of the lower Amazon basin (Rios Negro, Madeira/Jamari and Tapajós; but not including the Solimões) and reported Rio Negro-specific high molecular weight (>500 Da) signals. Besides some contributions of aromatic compounds below 300 Da, we found a similar signature in this study (centered at ~400 Da; Supplementary Fig. S17), although river signatures were rather similar. The data of Gonsior and coworkers differ from ours especially in the number of compounds containing N (besides C, H, and O), reporting average numbers of 1300–2100 detected CHNO formulae. The numbers of CHOS and CHO formulae agree well with our findings. For example, average (±SD) numbers of formulae detected in the MIX NF set were: 3225 (±102, CHO), 746 (±98, CHNO) and 291 (±9, CHOS). Larger differences among sampled rivers may relate to the larger spatial extent sampled, reflecting even larger climatic and geographical differences among watersheds.

The differences in higher *m*/*z*-specific molecular formulae and in numbers of CHNO formulae in Rio Negro waters could be explained by several aspects. First, Gonsior et al. (2016) did not make use of source-induced fragmentation (SID, personal communication, M. Gonsior), whereas this is a routine step in our measurement protocol in order to suppress dimer formation in the ESI source (40 eV). Tests with standard compounds have shown that this does not lead to fragmentation of single molecules (Waska et al., 2016; Zark and Dittmar, 2018). Second, the authors included floodplain lakes that are characterized by longer water residence time, seasonal disconnection, and higher OM inputs (allochthonous and autochthonous; Mortillaro et al., 2011; Moreira-Turcq et al., 2013).

Moreira-Turcq et al. (2003b) also show that DOC (and POC) fluxes are affected by higher water level for five main tributaries of the Amazon including the Rio Negro (increase of 50% in DOC flux during high water vs low water period) and Rio Solimões (increase of >100%). It can be expected that the number of molecular formulae and probably also the number of CHNO compounds would be affected by season (i.e., daily vs sparse precipitation, and water level variations), even more so as Gonsior et al. (2016) took their samples in May 2013, after the end of the rain season ("hot and wet", daily precipitation events) and the beginning maximum of the flood pulse (Vidal et al., 2015). The start of the flood peak will presumably differ largely from its end (initial disturbance vs ongoing/ending disturbance), for example in terms of dissolved constituents leached from rewetted soils. In comparison, the samples from this study were taken during the dry period ("hot and humid", non-daily precipitation), at the end of the maximum of the flood peak (July 2014) and its lowest extent (October 2013), when connectivity between floodplains and mainstem gradually decreases and upstream flushing of soils by daily precipitation events is reduced (see Supplementary Figs. S1 and S2 and Supplementary Note S1).

4.4. The non-conservative component of mixing

The ordination and gradient fitting (Fig. 6b–d) showed that there were other controlling factors besides mixing, but only few formulae were affected (87 formulae correlated negatively and 69 positively to coordinate 2, Fig. 8b). Iron and Cu showed distinct non-conservative behavior under particle influence, indicating desorption of Cu and alternating desorption and adsorption of Fe along the mixing line (Fig. 2b and c). The post-ordination gradient fitting of the MIX NF data set revealed that Cu, PEP compounds and partly also aromatic moieties (PP and BC compounds) correlated with coordinate 2 (i.e., non-conservative component), while most other parameters were correlated to coordinate 1 (i.e., conservative component, Fig. 6a–c). This effect was linked to the presence of particles, pointing toward surface phenomena being responsible for non-conservative effects (compare Fig. 7a–c). The intensity change when particles were absent (Fig. 7c) points toward a general response of PEP-type formulae upon mixing, while diversity-related (number of molecular formulae) changes only occurred under MIX NF conditions and in parallel to Cu release (Fig. 6b).

PEP compounds exhibited a distinct mixing response, showing a release below f = 0.5 and a depletion above f = 0.5, and were negatively correlated with d.Cu (based on the number of molecular formulae, Fig. 10a). The PEP mixing response suggests opposed sorption and desorption reactions that prevail when no particles are present (Supplementary Note S7), pointing towards effects related to changes in pH or conductivity (Spitzy and Leenheer, 1991). We note that we cannot exclude the effect of heterotrophic microbial processing during this experiment, including an equilibration step with continuous shaking for 24 h at room temperature under dark conditions (Ward et al., 2018).

The different mixing curves – the PEP one in particular – may thus also point towards processing that would also affect particle coatings during the experiment. However, we also note that the mixing behavior was observed in absence of particles, and that comparisons of differential mass spectra (Supplemental Fig. S19) indicated no systematic shifts in DOM composition in between MIX experiments and after shaking, as observed in similar experiments (Ward et al., 2013, Supplementary Note S5). If particles played a major role in determining DOM composition, we would have expected stronger differences between the non-filtered and filtered endmember samples after 24 h of shaking. If microbial processing affected DOM and trace metal levels, which we cannot exclude here, it did so independent of the presence of particles >0.2 μm.

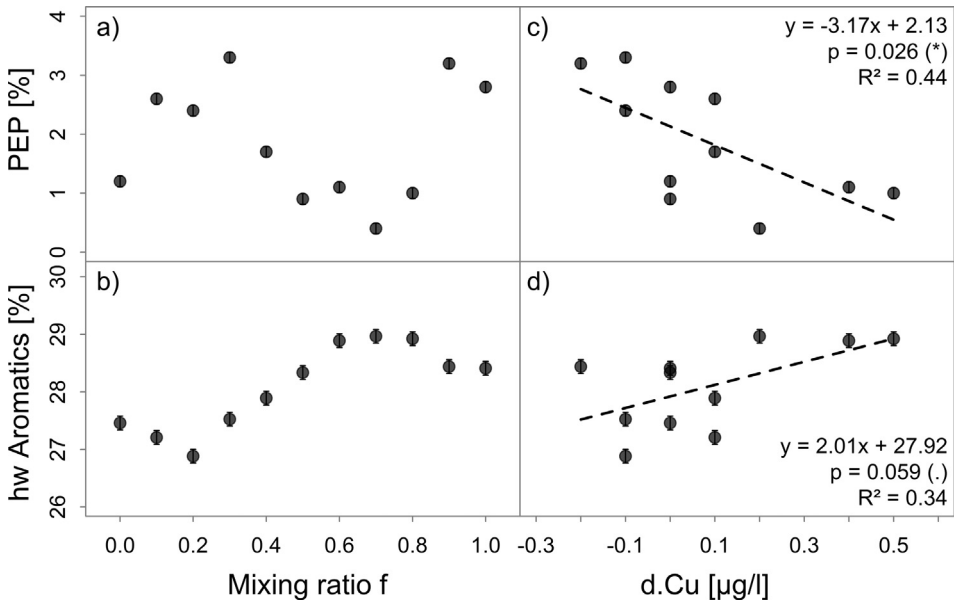

Fig. 10. Mixing behavior of the molecular groups of: (a) PEP formulae and (b) polyphenols and black carbon-like compounds is linked to Cu release (panels c and d, respectively) in the MIX NF experiment. Aromatic compounds with ≥ 15 C atoms (hwBC, polycyclic, condensed aromatics, such as "black carbon" and hwPP, polyphenols) were summed up. The PEP group of unsaturated, O- and N-containing compounds also includes compounds with < 2 N, strictly being non-peptides. Error bars are ± 1 SD estimated from repeated measurements of a eutrophic lake reference sample. Significance levels are denoted with (*) $p < 0.05$ and (.) $p < 0.1$.

The release of Cu in the mixing range f = 0.6–0.8 (Fig. 2c) was correlated with an increase in number of aromatic formulae (hwPP and hwBC, Fig. 10b and d, summed up as "hw aromatics"), which may point to mechanistic links between Cu release and this group of compounds (Supplementary Note S7). Desorption due to pH decrease could explain release of Cu (Rio Negro dominance, f = 0.6–0.8, Gaillardet et al., 2014). Lu and Allen (2001) state that the sorption of Cu occurs at pH > 6 (pH range observed was 3–8). The typical pH range in the Amazon confluence is pH 5–7 (Furch and Junk, 1997). DOC content and pH exert the major controls on Cu partitioning onto riverine DOC-conditioned suspended particulate matter (SPM) (Lu and Allen, 2001). Copper is also the divalent cation with strongest affinities to DOM (Xue and Sigg, 2002; Ksionzek et al., 2018). In a follow-up study, Lu and Allen (2002) found small amounts of strong phenolic Cu binding sites in DOM based on titration data. Although phenolic compartments in DOM were assessed in two different ways, the overall findings of these authors support the hypothesis that Cu release is linked to phenolic/aromatic-type formulae.

Polyphenols or phenolic entities in DOM are potential candidates for complex formation (Ross et al., 2000; Croué et al., 2003; Paunovic et al., 2005), and so is terrestrial DOM in general (Shank et al., 2004a, 2004b; Krachler et al., 2015). The mechanistic experiments of Lu and Allen (2001, 2002) were conducted under highly controlled conditions that do not match the exact conditions of the Amazon confluence, and further experiments would be needed to disentangle the in situ effects of pH, ion strength, DOC composition and sorption onto Cu partitioning, especially at full occupation of sorption sites (Kleber et al., 2007; Brown and Calas, 2012; Vogel et al., 2014). Lu and Allen (2001) did not observe a redissolution of once-sorbed DOC upon pH changes, in line with our bulk DOC observations including natural particles. DOC release from particles has been described by others (Keil et al., 1997; Avneri-Katz et al., 2017), but may be largely independent from ligand dynamics. The ligands controlling trace metal dynamics are likely below the detection limit or within the analytical error of most TOC analyzers at natural concentrations. The additional resolution via FT-ICRMS confirmed the conservative behavior of a major fraction of DOM compounds in our study (as discussed above), but indicated also non-conservative behavior.

Indeed, by application of CLE-AdCSV we were able to confirm the presence of strong ligands with a maximal binding capacity of about 3 µg Cu/L in the Rio Negro sample (NAT 08; see Supplementary Fig. S5 and Note S3). We also observed Fe-specific ligands that were not outcompeted by 1-nitroso-2-naphthol in reverse titration CLE-AdCSV (equivalent to 60 µg Fe/L in Rio Negro and 69 µg/L in Rio Solimões, see Supplementary Note S7 for more details). High complexation capacities exceeding the actual metal concentration have also been reported from other organic-rich rivers, as the Black River and Northeast Cape Fear River in North Carolina, USA (Shank et al., 2004b) and Xue et al. (1996) describe organic complexation rates of >99% for Cu in Swiss alpine lakes and rivers. Powell and Wilson-Finelli (2003) and Buck et al. (2007) describe Fe ligand concentrations exceeding dissolved Fe concentration in the plumes of the Mississippi River and Columbia River/San Francisco Bay. It can be expected that a large part of Fe is also controlled by strong Fe ligands in freshwater settings, especially in blackwater rivers (Jones et al., 2011), and our CLE-AdCSV data support this (Supplementary Note S7). These data are also in line with results from Electron Paramagnetic Resonance (EPR) spectroscopy presented by Mulholland et al. (2015) which show evidence for a differential mixing behavior of organically complexed Fe, as compared to other Fe pools (Supplementary Note S7).

Even though our study cannot draw direct links between the groups of PP, BC and PEP compounds and the behavior of trace metals Cu and Fe, their responses may indicate effects that are not readily observable by the chosen methodology. PPL generally extracts a wide range of highly polar to non-polar substances (Dittmar et al., 2008; Li et al., 2017), but it is known that solid phase sorbents characterized by a major portion of hydrophobic functionalities may be biased in that they do not retain small charged and neutral molecules (Repeta, 2015; Hawkes et al., 2016). For example, Sleighter and Hatcher (2008) demonstrated that C18-extracted blackwater samples were depleted in tannin- and peptide-type formulae. In a subsequent study, these authors showed that the discriminated molecules were more hydrophilic,

of lower molecular weight and likely enriched in bound metals (Liu et al., 2011).

As with other analytical techniques, the combination of SPE and ESI-FT-ICRMS has its specific analytical window and does not cover the entire spectrum of dissolved organic molecules (Hawkes et al., 2016; Raeke et al., 2016). It is, however, the most comprehensive technique providing DOM molecular information in unsurpassed detail and an effective tool to study unknown metal ligands in DOM (Waska et al., 2015, 2016). Cu and Fe behavior could be connected to molecular groups that were not addressed by our method. Future studies could close the gap, for instance through parallel or sequential IMAC (immobilized metal-ion affinity chromatography) protocols that are able to retain metal-specific ligands (Paunovic et al., 2005; Smith et al., 2014), or direct measurement of trace metals in DOM extracts (both in retentate and permeate, Waska et al., 2015; Ksionzek et al., 2018).

Both Boiteau et al. (2016) and Kügler et al. (2019) found Cu and Fe ligands in marine and terrestrial settings, respectively, by making use of characteristic isotope patterns and ultrahigh resolution MS techniques combined with prior LC separation. It is not surprising that the search for these specific patterns ($^{63}Cu/^{65}Cu$ and $^{54}Fe/^{56}Fe$) in our direct-injection broadband FT-ICRMS data was unsuccessful. Cu and Fe ligand detection under natural concentrations may require narrower acquisition windows (m/z window; hence enhancing sensitivity), measurements in positive ESI mode (Waska et al., 2015; hence enhancing selectivity), or prior separation (hence reducing complexity). In this regard, isotope labeling approaches with the respective metals could help to better capture trace metal-DOM interactions by mass spectrometry (Wiederhold, 2015; Wichard, 2016).

5. Conclusions

We have shown that the Rio Negro is not only an important source of aromatic compounds to the Amazon, but also that most of these compounds show low reactivity during formation of the Amazon River through mixing with the Rio Solimões. The abundance of low-molecular mass aromatics in Rio Negro waters indicates fast transit of fresh or freshly degraded DOM from soil environments with lower sorptive capacities in its catchment. Non-conservative effects of both trace metals Fe and Cu were only observed in the presence of natural particles and were not reflected by the majority of DOM molecular formulae. The surprisingly low reactivity of bulk DOM under experimental conditions indicates that the dynamics of trace metals might be governed by small amounts of highly specific ligands not readily observable by our methodology. A small number of molecular formulae indeed showed a differential response: Polyphenols were positively linked to Cu release only when natural particles >0.2 μm were present, pointing towards potential Cu ligands, and N-containing compounds showed a general response in signal abundance likely induced by pH and conductivity changes controlling charge properties of these compounds. Our first results on Cu and Fe complexation by DOM in the Amazon confluence system stress the importance of electrochemical analyses, as CLE-AdCSV, for the study of trace metal dynamics and DOC-borne metal-specific ligands in natural waters. FT-ICRMS is able to capture non-conservative processes in unsurpassed detail, but the dynamics and identity of metal ligands in the DOM pool need to be further studied with adjusted methods that are more selective and sensitive. The largely conservative behavior of DOM contrasts with previous findings that often presume a major role of organic compounds in non-conservative processes. According to our findings, non-conservative effects likely vary in space and time and can be smaller than expected. Taking into account that more than 80% of river length of the Amazon River network is connected to small streams, it seems certain that the impact and temporal dynamics of upstream processes within smaller tributaries and lower order confluences or at the soil/water interface may have been overlooked in the past and will need reconsideration.

Acknowledgments

We thank Gila Merschel, Sandra Pöhle, Inken Preuss, Clive Maguire and Florian Wittmann (INPA/MPI Manaus) for their support of the field sampling trip on the Amazon. Travel funds for the field trip were provided through the DAAD exchange program PROBRAL 54393165. Bernhard Schnetger and Eleonore Gründken enabled ICP-MS access at ICBM, Oldenburg and helped in the course of laboratory work, data acquisition/processing and interpretation. Stefan Kuzmanovski and Ann Noowong are acknowledged for CLE-AdCSV measurements and data processing, and Charlotte Kleint and Jule Mawick are thanked for support in the laboratory in Bremen. Katrin Klaproth and Ina Ulber are acknowledged for their support and advice in the laboratory and during FT-ICRMS measurements. Marcus Manecki, Thomas Riedel and Benjamin Jacob are acknowledged for providing Matlab and R routines. Hannelore Waska, Jomar S.J. Marques and Vanessa-Nina Roth contributed valuable comments on earlier versions of the manuscript. Hydrological data from the CAMREX project were obtained from the Oak Ridge National Laboratory Distributed Active Archive Center (ORNL DAAC) for biogeochemical dynamics (http://daac.ornl.gov/), and for the years 2013 and 2014 from Serviço Geológico do Brasil (http://www.cprm.gov.br/). Carsten Simon received financial support through a PhD stipend from the International Max Planck Research School for Global Biogeochemical Cycles (IMPRS-gBGC) and as a member of CRC 1076 "AquaDiva" funded by the German Research Foundation (DFG). Finally, the authors want to thank the Editor-in-chief, Dr. John Volkman, and Associate Editor Dr. Elizabeth Minor, and three anonymous reviewers for their dedication and useful comments, requests and suggestions that helped to improve this work substantially.

Appendix A. Supplementary material

Supplementary data to this article can be found online at https://doi.org/10.1016/j.orggeochem.2019.01.013.

Associate Editor—**Elizabeth Minor**

References

Abril, G., Martinez, J.-M., Artigas, L.F., Moreira-Turcq, P., Benedetti, M.F., Vidal, L., Meziane, T., Kim, J.-H., Bernardes, M.C., Savoye, N., Deborde, J., Souza, E.L., Albéric, P., Landim de Souza, M.F., Roland, F., 2014. Amazon River carbon dioxide outgassing fueled by wetlands. Nature 505, 395–398.

Affonso, A.G., Queiroz, H.L., Novo, E.M.L.M., 2015. Abiotic variability among different aquatic systems of the central Amazon floodplain during drought and flood events. Brazilian Journal of Biology 75, 60–69.

Asmala, E., Kaartokallio, H., Carstensen, J., Thomas, D.N., 2016. Variation in riverine inputs affect dissolved organic matter characteristics throughout the estuarine gradient. Frontiers in Marine Science 2, 125.

Aucour, A.-M., Tao, F.-X., Moreira-Turcq, P., Seyler, P., Sheppard, S., Benedetti, M.F., 2003. The Amazon River: behaviour of metals (Fe, Al, Mn) and dissolved organic matter in the initial mixing at the Rio Negro/Solimões confluence. Chemical Geology 197, 271–285.

Aufdenkampe, A.K., Hedges, J.I., Richey, J.E., Krusche, A.V., Llerena, C.A., 2001. Sorptive fractionation of dissolved organic nitrogen and amino acids onto fine sediments within the Amazon Basin. Limnology and Oceanography 46, 1921–1935.

Aufdenkampe, A.K., Mayorga, E., Raymond, P.A., Melack, J.M., Doney, S.C., Alin, S.R., Aalto, R.E., Yoo, K., 2011. Riverine coupling of biogeochemical cycles between land, oceans, and atmosphere. Frontiers in Ecology and the Environment 9, 53–60.

Avneri-Katz, S., Young, R.B., McKenna, A.M., Chen, H., Corilo, Y.E., Polubesova, T., Borch, T., Chefetz, B., 2017. Adsorptive fractionation of dissolved organic matter

(DOM) by mineral soil: macroscale approach and molecular insight. Organic Geochemistry 103, 113–124.
Bardy, M., Derenne, S., Allard, T., Benedetti, M.F., Fritsch, E., 2011. Podzolisation and exportation of organic matter in black waters of the Rio Negro (upper Amazon Basin, Brazil). Biogeochemistry 106, 71–88.
Battin, T.J., Luyssaert, S., Kaplan, L.A., Aufdenkampe, A.K., Richter, A., Tranvik, L.J., 2009. The boundless carbon cycle. Nature Geoscience 2, 598–600.
Boiteau, R.M., Till, C.P., Ruacho, A., Bundy, R.M., Hawco, N.J., McKenna, A.M., Barbeau, K.A., Bruland, K.W., Saito, M.A., Repeta, D.J., 2016. Structural characterization of natural nickel and copper binding ligands along the US GEOTRACES Eastern Pacific zonal transect. Frontiers in Marine Science 3, 243. https://doi.org/10.3389/fmars.2016.00243.
Brown, G.E., Calas, G., 2012. Sorption reactions in more complex model systems: containing NOM and microbial biofilm coatings. In: Brown, G.E., Calas, G. (Eds.), Mineral-Aqueous Solution Interfaces and Their Impact on the Environment. Geochemical Perspectives 1, No. 4–5, pp. 603–610.
Buck, K.N., Lohan, M.C., Berger, C.J.M., Bruland, K.M., 2007. Dissolved iron speciation in two distinct river plumes and an estuary: implications for riverine iron supply. Limnology and Oceanography 52, 843–855.
Buck, K.N., Moffett, J., Barbeau, K.A., Bundy, R.M., Kondo, Y., Wu, J., 2012. The organic complexation of iron and copper: an intercomparison of competitive ligand exchange – adsorptive cathodic stripping voltammetry (CLE-ACSV) techniques. Limnology and Oceanography: Methods 10, 496–515.
Cifuentes, L.A., Schemel, L.E., Sharp, J.H., 1990. Qualitative and numerical analyses of the effects of river inflow variations on mixing diagrams in estuaries. Estuarine, Coastal and Shelf Science 30, 411–427.
Coynel, A., Seyler, P., Etcheber, H., Meybeck, M., Orange, D., 2005. Spatial and seasonal dynamics of total suspended sediment and organic carbon species in the Congo River. Global Biogeochemical Cycles 19, 1–17.
Croué, J.P., Benedetti, M.F., Violleau, D., Leenheer, J.A., 2003. Characterization and copper binding of humic and nonhumic organic matter isolated from the South Platte River: evidence for the presence of nitrogenous binding site. Environmental Science and Technology 37, 328–336.
Dai, M., Yin, Z., Meng, F., Liu, Q., Cai, W.-J., 2012. Spatial distribution of riverine DOC inputs to the ocean: an updated global synthesis. Current Opinion in Environmental Sustainability 4, 170–178.
Davis, J.A., 1982. Adsorption of natural dissolved organic matter at the oxide/water interface. Geochimica et Cosmochimica Acta 46, 2381–2393.
Devol, A.H., Hedges, J.I., 2001. Organic matter and nutrients in the mainstem Amazon River. In: McClain, M.E., Victoria, R.L., Richey, J.E. (Eds.), The Biogeochemistry of the Amazon Basin. Oxford University Press, Oxford, pp. 275–365.
Dittmar, T., Koch, B., Hertkorn, N., Kattner, G., 2008. A simple and efficient method for the solid-phase extraction of dissolved organic matter (SPE-DOM) from seawater. Limnology and Oceanography: Methods 6, 230–235.
Ertel, J.R., Hedges, J.I., Devol, A.H., Richey, J.E., De Nazaré Goés Ribeiro, M., 1986. Dissolved humic substances of the Amazon River system. Limnology and Oceanography 31, 739–754.
Farjalla, V.F., 2014. Are the mixing zones between aquatic ecosystems hot spots of bacterial production in the Amazon River system? Hydrobiologia 728, 153–165.
Filizola, N., Spínola, N., Arruda, W., Seyler, F., Calmant, S., Silva, J., 2010. The Rio Negro and Rio Solimões confluence point – hydrometric observations during the 2006/2007 cycle. In: Vionnet, C., García, M.H., Latrubesse, E.M., Perillo, G.M. E. (Eds.), River, Coastal and Estuarine Morphodynamics RCEM 2009. Taylor and Francis, London, pp. 1003–1006.
Fritsch, E., Allard, T., Benedetti, M.F., Bardy, M., do Nascimento, N.R., Li, Y., Calas, G., 2009. Organic complexation and translocation of ferric iron in podzols of the Negro River watershed. Separation of secondary Fe species from Al species. Geochimica et Cosmochimica Acta 73, 1813–1825.
Furch, K., Junk, W.J., 1997. Physicochemical conditions in floodplains. In: Junk, W.J. (Ed.), The Central Amazon Floodplain. Ecology of a Pulsing System. Ecological Studies 126. Springer, Heidelberg, pp. 69–108.
Gaillardet, J., Viers, J., Dupré, B., 2014. Trace elements in river waters. In: Holland, H., Turekian, K., Drever, J.I. (Eds.), Treatise on Geochemistry. Second edition. Volume 7: Surface and Groundwater, Weathering and Soils. Elsevier, Oxford, pp. 195–235.
Gonsior, M., Valle, J., Schmitt-Kopplin, P., Hertkorn, N., Bastviken, D., Luek, J., Harir, M., Bastos, W., Enrich-Prast, A., 2016. Chemodiversity of dissolved organic matter in the Amazon Basin. Biogeosciences 13, 4279–4290.
Guinoiseau, D., Bouchez, J., Gélabert, A., Louvat, P., Filizola, N., Benedetti, M.F., 2016. The geochemical filter of large river confluences. Chemical Geology 441, 191–203.
Guinoiseau, D., Gélabert, A., Allard, T., Louvat, P., Moreira-Turcq, P., Benedetti, M.F., 2017. Zinc and copper behavior at the soil-river interface: new insights by Zn and Cu isotopes in the organic-rich Rio Negro basin. Geochimica et Cosmochimica Acta 213, 178–197.
Guinoiseau, D., Bouchez, J., Gélabert, A., Louvat, P., Moreira-Turcq, P., Filizola, N., Benedetti, M.F., 2018. Fate of particulate copper and zinc isotopes at the Solimões-Negro river confluence, Amazon Basin, Brazil. Chemical Geology 489, 1–15.
Hawkes, J.A., Gledhill, M., Connelly, D.P., Achterberg, E.P., 2013. Characterisation of iron binding ligands in seawater by reverse titration. Analytica Chimica Acta 766, 53–60.
Hawkes, J.A., Hansen, C.T., Goldhammer, T., Bach, W., Dittmar, T., 2016. Molecular alteration of marine dissolved organic matter under experimental hydrothermal conditions. Geochimica et Cosmochimica Acta 175, 68–85.
Irion, G., 1991. Minerals in rivers. In: Degens, E., Kempe, S., Richey, J. (Eds.), SCOPE 42 – Biogeochemistry of Major World Rivers. John Wiley and Sons, Chichester, pp. 265–282.
Johannsson, O.E., Smith, D.S., Sadauskas-Henrique, H., Cimprich, G., Wood, C.M., Val, A.L., 2016. Photo-oxidation processes, properties of DOC, reactive oxygen species (ROS), and their potential impacts on native biota and carbon cycling in the Rio Negro (Amazonia, Brazil). Hydrobiologia 789, 7–29.
Jones, M.E., Beckler, J.S., Taillefert, M., 2011. The flux of soluble organic-iron (III) complexes from sediments represents a source of stable iron(III) to estuarine waters and to the continental shelf. Limnology and Oceanography 56, 1811–1823.
Jost, L., 2006. Entropy and diversity. OIKOS 113, 363–375.
Junk, W.J., Piedade, M.T.F., Schöngart, J., Cohn-Haft, M., Adeney, J.M., Wittmann, F., 2011. A classification of major naturally-occurring Amazonian lowland wetlands. Wetlands 31, 623–640.
Keil, R.G., Mayer, L.M., Quay, P.D., Richey, J.E., Hedges, J.I., 1997. Loss of organic matter from riverine particles in deltas. Geochimica et Cosmochimica Acta 61, 1507–1511.
Kleber, M., Sollins, P., Sutton, R., 2007. A conceptual model of organo-mineral interactions in soils: self-assembly of organic molecular fragments into zonal structures on mineral surfaces. Biogeochemistry 85, 9–24.
Kleint, C., Kuzmanovski, S., Powell, Z., Bühring, S.I., Sander, S.G., Koschinsky, A., 2015. Organic Cu-complexation at the shallow marine hydrothermal vent fields off the coast of Milos (Greece), Dominica (Lesser Antilles) and the Bay of Plenty (New Zealand). Marine Chemistry 173, 244–252.
Koch, B.P., Dittmar, T., 2006. From mass to structure: an aromaticity index for high-resolution mass data of natural organic matter. Rapid Communications in Mass Spectrometry 20, 926–932.
Koch, B.P., Dittmar, T., 2016. Erratum to: From mass to structure: an aromaticity index for high-resolution mass data of natural organic matter. Rapid Communications in Mass Spectrometry 30, 250.
Koch, B.P., Dittmar, T., Witt, M., Kattner, G., 2007. Fundamentals of molecular formula assignment to ultrahigh resolution mass data of natural organic matter. Analytical Chemistry 79, 1758–1763.
Krachler, R., Krachler, R.F., Wallner, G., Hann, S., Laux, M., Cervantes Recalde, M.F., Jirsa, F., Neubauer, E., von der Kammer, F., Hofmann, T., Keppler, B.K., 2015. River-derived humic substances as iron chelators in seawater. Marine Chemistry 174, 85–93.
Ksionzek, K.B., Zhang, J., Ludwichowski, K.-U., Wilhelms-Dick, D., Trimborn, S., Jendrossek, T., Kattner, G., Koch, B.P., 2018. Stoichiometry, polarity, and organometallics in solid-phase extracted dissolved organic matter of the Elbe-Weser estuary. PLoS ONE 13 (9), e0203260.
Küchler, I.L., Miekeley, N., Forsberg, B.R., 1994. Molecular mass distributions of dissolved organic carbon and associated metals in waters from Rio Negro and Rio Solimões. Science of the Total Environment 156, 207–216.
Kügler, S., Cooper, R.E., Wegner, C.-E., Mohr, J.F., Wichard, T., Küsel, K., 2019. Iron-organic matter complexes accelerate microbial iron cycling in an iron-rich fen. Science of the Total Environment 646, 972–988.
Kujawinski, E.B., 2011. The impact of microbial metabolism on marine dissolved organic matter. Annual Review of Marine Science 3, 567–599.
Kuzyakov, Y., Blagodatskaya, E., 2015. Microbial hotspots and hot moments in soil: concept & review. Soil Biology and Biochemistry 83, 184–199.
Laane, R.W.P.M., 1980. Conservative behaviour of dissolved organic carbon in the Ems-Dollart estuary and the Western Wadden Sea. Netherlands Journal of Sea Research 14, 192–199.
Laraque, A., Guyot, J.L., Filizola, N., 2009. Mixing processes in the Amazon River at the confluences of the Negro and Solimões Rivers, Encontro das Águas, Manaus, Brazil. Hydrological Processes 23, 3131–3140.
Leenheer, J.A., Menezes Santos, U., 1980. Considerações sobre os processos de sedimentaçãao na agua preta acida do Rio Negro (Amazônica Central). Acta Amazonica 10, 343–355.
Li, Y., Harir, M., Uhl, J., Kanawati, B., Lucio, M., Smirnov, K.S., Koch, B.P., Schmitt-Kopplin, P., Hertkorn, N., 2017. How representative are dissolved organic matter (DOM) extracts? A comprehensive study of sorbent selectivity for DOM isolation. Water Research 116, 316–323.
Liu, Z., Sleighter, R.L., Zhong, J., Hatcher, P.G., 2011. The chemical changes of DOM from black waters to coastal marine waters by HPLC combined with ultrahigh resolution mass spectrometry. Estuarine, Coastal and Shelf Science 92, 205–216.
Loder, T.C., Reichard, R.P., 1981. The dynamics of conservative mixing in estuaries. Estuaries 4, 64–69.
Longnecker, K., Kido Soule, M.C., Kujawinski, E.B., 2015. Dissolved organic matter produced by *Thalassiosira pseudonana*. Marine Chemistry 168, 114–123.
Lu, Y., Allen, H.E., 2001. Partitioning of copper onto suspended particulate matter in river waters. Science of the Total Environment 277, 119–132.
Lu, Y., Allen, H.E., 2002. Characterization of copper complexation with natural dissolved organic matter (DOM) – Link to acidic moieties of DOM and competition by Ca and Mg. Water Research 36, 5083–5101.
Mantoura, R.F.C., Woodward, E.M.S., 1983. Conservative behavior of riverine dissolved organic carbon In the Severn Estuary – chemical and geochemical implications. Geochimica et Cosmochimica Acta 47, 1293–1309.
Marín-Spiotta, E., Gruley, K.E., Crawford, J., Atkinson, E.E., Miesel, J.R., Greene, S., Cardona-Correa, C., Spencer, R.G.M., 2014. Paradigm shifts in soil organic matter research affect interpretations of aquatic carbon cycling: transcending disciplinary and ecosystem boundaries. Biogeochemistry 117, 279–297.
Mayorga, E., Aufdenkampe, A.K., Masiello, C.A., Krusche, A.V., Hedges, J.I., Quay, P.D., Richey, J.E., Brown, T.A., 2005. Young organic matter as a source of carbon dioxide outgassing from Amazonian rivers. Nature 436, 538–541.

McClain, M.E., Elsenbeer, H., 2001. Terrestrial inputs to Amazon streams and internal biogeochemical processing. In: McClain, M.E., Victoria, R., Richey, J.E. (Eds.), The Biogeochemistry of the Amazon Basin. Oxford University Press, New York, pp. 185–208.

McKnight, D.M., Bencala, K.E., Zellweger, G.W., Aiken, G.R., Feder, G.L., Thorn, K.A., 1992. Sorption of dissolved organic carbon by hydrous aluminum and iron oxides occurring at the confluence of Deer Creek with the Snake River, Summit County, Colorado. Environmental Science and Technology 26, 1388–1396.

Mentges, A., Feenders, C., Seibt, M., Blasius, B., Dittmar, T., 2017. Functional molecular diversity of marine dissolved organic matter is reduced during degradation. Frontiers in Marine Science 4, 194. https://doi.org/10.3389/fmars.2017.00194.

Merschel, G., Bau, M., Dantas, E.L., 2017. Contrasting impact of organic and inorganic nanoparticles and colloids on the behavior of particle-reactive elements in tropical estuaries: an experimental study. Geochimica et Cosmochimica Acta 197, 1–13.

Moreira-Turcq, P.F., Seyler, P., Guyot, J.L., Etcheber, H., 2003a. Characteristics of organic matter in the mixing zone of the Rio Negro and Rio Solimões of the Amazon River. Hydrological Processes 17, 1393–1404.

Moreira-Turcq, P.F., Seyler, P., Guyot, J.L., Etcheber, H., 2003b. Exportation of organic carbon from the Amazon River and its main tributaries. Hydrological Processes 17, 1329–1344.

Moreira-Turcq, P.F., Bonnet, M.-P., Amorim, M., Bernardes, M., Lagane, C., Maurice, L., Pérez, M.A.P., Seyler, P., 2013. Seasonal variability in concentration, composition, age, and fluxes of particulate organic carbon exchanged between the floodplain and Amazon River. Global Biogeochemical Cycles 27, 119–130.

Mortillaro, J.M., Abril, G., Moreira-Turcq, P.F., Sobrinho, R.L., Pérez, M.A.P., Meziane, T., 2011. Fatty acid and stable isotope ($\delta^{13}C$, $\delta^{15}N$) signatures of particulate organic matter in the lower Amazon River: seasonal contrasts and connectivity between floodplain lakes and the mainstem. Organic Geochemistry 42, 1159–1168.

Mulholland, D.S., Poitrasson, F., Boaventura, G.R., Allard, T., Vieira, L.C., Santos, R.V., Mancini, L., Seyler, P., 2015. Insights into iron sources and pathways in the Amazon River provided by isotopic and spectroscopic studies. Geochimica et Cosmochimica Acta 150, 142–159.

Oksanen, J., 2015. Multivariate analysis of ecological communities in R: vegan tutorial. URL: http://www.cc.oulu.fi/~jarioksa/opetus/metodi/vegantutor.pdf. Version from 10-06-2015. Last accessed on 10-01-2019.

Palmer, S.M., Evans, C.D., Chapman, P.J., Burden, A., Jones, T.G., Allott, T.E.H., Evans, M.G., Moody, C.S., Worrall, F., Holden, J., 2015. Sporadic hotspots for physico-chemical retention of aquatic organic carbon: from peatland headwater source to sea. Aquatic Sciences 78, 491–504.

Paunovic, I., Schulin, R., Nowack, B., 2005. Evaluation of immobilized metal-ion affinity chromatography for the fractionation of natural Cu complexing ligands. Journal of Chromatography A 1100, 176–184.

Pérez, M.A.P., Moreira-Turcq, P., Gallard, H., Allard, T., Benedetti, M.F., 2011. Dissolved organic matter dynamic in the Amazon Basin: sorption by mineral surfaces. Chemical Geology 286, 158–168.

Powell, R.T., Wilson-Finelli, A., 2003. Importance of organic Fe complexing ligands in the Mississippi River plume. Estuarine, Coastal and Shelf Science 58, 757–763.

Quesada, C.A., Lloyd, J., Anderson, L.O., Fyllas, N.M., Schwarz, M., Czimczik, C.I., 2011. Soils of Amazonia with particular reference to the RAINFOR sites. Biogeosciences 8, 1415–1440.

Raeke, J., Lechtenfeld, O.J., Wagner, M., Herzsprung, P., Reemtsma, T., 2016. Selectivity of solid phase extraction of freshwater dissolved organic matter and its effect on ultrahigh resolution mass spectra. Environmental Science: Processes and Impacts 18, 918–927.

Ramette, A., 2007. Multivariate analyses in microbial ecology. FEMS Microbiology Ecology 62, 142–160.

Repeta, D.J., 2015. Chemical characterization and cycling of dissolved organic matter. In: Hansell, D.A., Carlson, C.A. (Eds.), Biogeochemistry of Marine Dissolved Organic Matter. Elsevier, London, pp. 21–63.

Rice, S.P., Kiffney, P., Greene, C., Pess, G.E., 2008. The ecological importance of tributaries and confluence. In: Rice, S.P., Roy, A.G., Rhoads, B.L. (Eds.), River Confluences, Tributaries and the Fluvial Network. John Wiley and Sons, pp. 209–242.

Richey, J.E., Mertes, L.A.K., Dunne, T., Victoria, R.L., Forsberg, B.R., Tancredi, A.C.N.S., Oliveira, E., 1989. Sources and routing of the Amazon River flood wave. Global Biogeochemical Cycles 3, 191–204.

Riedel, T., Zak, D., Biester, H., Dittmar, T., 2013. Iron traps terrestrially derived dissolved organic matter at redox interfaces. Proceedings of the National Academy of Sciences 110, 10101–10105.

Riedel, T., Dittmar, T., 2014. A method detection limit for the analysis of natural organic matter via Fourier transform ion cyclotron resonance mass spectrometry. Analytical Chemistry 86, 8376–8382.

Röpke, C.P., Amadio, S.A., Winemiller, K.O., Zuanon, J., 2016. Seasonal dynamics of the fish assemblage in a floodplain lake at the confluence of the Negro and Amazon rivers. Journal of Fish Biology 89, 194–212.

Ross, A.R.S., Ikonomou, M.G., Orians, K.J., 2000. Characterization of dissolved tannins and their metal-ion complexes by electrospray ionization mass spectrometry. Analytica Chimica Acta 411, 91–102.

Rossel, P.E., Bienhold, C., Boetius, A., Dittmar, T., 2016. Dissolved organic matter in pore water of Arctic Ocean sediments: environmental influence on molecular composition. Organic Geochemistry 97, 41–52.

Roth, V.-N., Dittmar, T., Gaupp, R., Gleixner, G., 2015. The molecular composition of dissolved organic matter in forest soils as a function of pH and temperature. PLoS ONE 10 (3), e0119188.

Roth, V.-N., Lange, M., Dittmar, T., Gleixner, G., 2016. Broadband molecular composition of dissolved organic matter in grassland soil as a function of depth. Geophysical Research Abstracts 18, 8840.

Šantl-Temkiv, T., Finster, K., Dittmar, T., Hansen, B.M., Thyrhaug, R., Woetmann Nielsen, N., Gosewinkel Karlson, U., 2013. Hailstones: a window into the microbial and chemical inventory of a storm cloud. PLoS One 8 (1), e53550.

Schneider, A.B., Koschinsky, A., Kiprotich, J., Poehle, S., do Nascimento, P.C., 2016. An experimental study on the mixing behavior of Ti, Zr, V and Mo in the Elbe, Rhine and Weser estuaries. Estuarine, Coastal and Shelf Science 170, 34–44.

Shank, G.C., Skrabal, S.A., Whitehead, R.F., Avery, G.B., Kieber, R.J., 2004a. River discharge of strong Cu-complexing ligands to South Atlantic Bight waters. Marine Chemistry 88, 41–51.

Shank, G.C., Skrabal, S.A., Whitehead, R.F., Kieber, R.J., 2004b. Strong copper complexation in an organic-rich estuary: the importance of allochthonous dissolved organic matter. Marine Chemistry 88, 21–39.

Shen, Y., Chapelle, F.H., Strom, E.W., Benner, R., 2015. Origins and bioavailability of dissolved organic matter in groundwater. Biogeochemistry 122, 61–78.

Sleighter, R.L., Hatcher, P.G., 2008. Molecular characterization of dissolved organic matter (DOM) along a river to ocean transect of the lower Chesapeake Bay by ultrahigh resolution electrospray ionization Fourier transform ion cyclotron resonance mass spectrometry. Marine Chemistry 110, 140–152.

Smith, C.L., Stauber, J.L., Wilson, M.R., Jolley, D.F., 2014. The use of immobilised metal affinity chromatography (IMAC) to compare expression of copper-binding proteins in control and copper-exposed marine microalgae. Analytical and Bioanalytical Chemistry 406, 305–315.

Spitzy, A., Leenheer, J., 1991. Dissolved organic carbon in rivers. In: Degens, E., Kempe, S., Richey, J. (Eds.), SCOPE 42 – Biogeochemistry of Major World Rivers. John Wiley and Sons, Chichester, pp. 213–232.

Stedmon, C.A., Markager, S., 2003. Behaviour of the optical properties of coloured dissolved organic matter under conservative mixing. Estuarine, Coastal and Shelf Science 57, 973–979.

Takahashi, Y., Minai, Y., Ambe, S., Makide, Y., Ambe, F., 1999. Comparison of adsorption behavior of multiple inorganic ions on kaolinite and silica in the presence of humic acid using the multitracer technique. Geochimica et Cosmochimica Acta 63, 815–836.

Vidal, L.O., Abril, G., Artigas, L.F., Melo, M.L., Bernardes, M.C., Lobão, L.M., Reis, M.C., Moreira-Turcq, P., Benedetti, M., Tornisielo, V.L., Roland, F., 2015. Hydrological pulse regulating the bacterial heterotrophic metabolism between Amazonian mainstems and floodplain lakes. Frontiers in Microbiology 6, 1–10.

Viers, J., Barroux, G., Pinelli, M., Seyler, P., Oliva, P., Dupré, B., Boaventura, G.R., 2005. The influence of the Amazonian floodplain ecosystems on the trace element dynamics of the Amazon River mainstem (Brazil). Science of the Total Environment 339, 219–232.

Vogel, C., Mueller, C., Höschen, C., Buegger, F., Heister, K., Schulz, S., Schloter, M., Kögel-Knabner, I., 2014. Submicron structures provide preferential spots for carbon and nitrogen sequestration in soils. Nature Communications 5, 1–7.

Waggoner, D.C., Chen, H., Willoughby, A.S., Hatcher, P.G., 2015. Formation of black carbon-like and alicyclic aliphatic compounds by hydroxyl radical initiated degradation of lignin. Organic Geochemistry 82, 69–76.

Waggoner, D.C., Hatcher, P.G., 2017. Hydroxyl radical alteration of HPLC fractionated lignin: formation of new compounds from terrestrial organic matter. Organic Geochemistry 113, 315–325.

Ward, N.D., Keil, R.G., Medeiros, P.M., Brito, D.C., Cunha, A.C., Dittmar, T., Yager, P.L., Krusche, A.V., Richey, J.E., 2013. Degradation of terrestrially derived macromolecules in the Amazon River. Nature Geoscience 6, 530–533.

Ward, N., Bianchi, T., Medeiros, P., Seidel, M., Richey, J., Keil, R., Sawakuchi, H., 2017. Where carbon goes when water flows: carbon cycling across the aquatic continuum. Frontiers in Ecology and the Environment 4, 1–27.

Ward, N.D., Sawakuchi, H.O., Neu, V., Less, D.F.S., Valerio, A.M., Cunha, A.C., Kampel, M., Bianchi, T.S., Krusche, A.V., Richey, J.E., Keil, R.G., 2018. Velocity-amplified microbial respiration rates in the lower Amazon River. Limnology and Oceanography Letters 3, 265–274.

Waska, H., Koschinsky, A., Dittmar, T., 2016. Fe- and Cu-complex formation with artificial ligands investigated by ultra-high resolution Fourier-transform ion cyclotron resonance mass spectrometry (FT-ICR-MS): implications for natural metal-organic complex studies. Frontiers in Marine Science 3, 1–19.

Waska, H., Koschinsky, A., Ruiz Chancho, M.J., Dittmar, T., 2015. Investigating the potential of solid-phase extraction and Fourier-transform ion cyclotron resonance mass spectrometry (FT-ICR-MS) for the isolation and identification of dissolved metal–organic complexes from natural waters. Marine Chemistry 173, 78–92.

Wichard, T., 2016. Identification of metallophores and organic ligands in the chemosphere of the marine macroalga *Ulva* (Chlorophyta) and at land-sea interfaces. Frontiers in Marine Science 3, 131. https://doi.org/10.3389/fmars.2016.00131.

Wiederhold, J.G., 2015. Metal stable isotope signatures as tracers in environmental geochemistry. Environmental Science and Technology 49, 2606–2624.

Xue, H., Oestreich, A., Kistler, D., Sigg, L., 1996. Free cupric ion concentrations and Cu complexation in selected Swiss lakes and rivers. Aquatic Sciences 58, 69–87.

Xue, H., Sigg, L., 2002. A review of competitive ligand-exchange – voltammetric methods for speciation of trace elements in freshwater. In: Taillefert, M., Rozan, T.F. (Eds.), Environmental Electrochemistry. Analyses of Trace Element

Biogeochemistry. ACS Symposium Series 811. Oxford University Press, Oxford, pp. 336–370.
Ylöstalo, P., Seppälä, J., Kaitala, S., Maunula, P., Simis, S., 2016. Loadings of dissolved organic matter and nutrients from the Neva River into the Gulf of Finland – biogeochemical composition and spatial distribution within the salinity gradient. Marine Chemistry 186, 58–71.
Zark, M., Dittmar, T., 2018. Universal molecular structures in natural dissolved organic matter. Nature Communications 9, 1–8.